Genomic analyses of Pamir argali, Tibetan sheep and their hybrids provide insights into chromosome evolution, phenotypic variation and germplasm innovation

Xin Li[1,2,3,13], San-Gang He[4,13], Wen-Rong Li[4,13], Ling-Yun Luo[1], Ze Yan[1], Dong-Xin Mo[1], Xing Wan[1], Feng-Hua Lv[1], Ji Yang[1], Ya-Xi Xu[1], Juan Deng[1,5], Qiang-Hui Zhu[1,2,3], Xing-Long Xie[2,3], Song-Song Xu[2,3], Chen-Xi Liu[4], Xin-Rong Peng[4], Bin Han[4], Zhong-Hui Li[4], Lei Chen[4], Jian-Lin Han[6,7], Xue-Zhi Ding[8], Renqing Dingkao[9], Yue-Feng Chu[10], Jin-Yan Wu[10], Li-Min Wang[11,12], Ping Zhou[11,12], Ming-Jun Liu[4*], Meng-Hua Li[1*]

[1]College of Animal Science and Technology, China Agricultural University, Beijing 100193, China

[2]CAS Key Laboratory of Animal Ecology and Conservation Biology, Institute of Zoology, Chinese Academy of Sciences (CAS), Beijing 100101, China

[3]College of Life Sciences, University of Chinese Academy of Sciences (UCAS), Beijing 100049, China

[4]MOA Key Laboratory of Ruminant Genetics, Breeding and Reproduction, Ministry of Agriculture (MOA), Key Laboratory of Animal Technology of Xinjiang, Xinjiang Academy of Animal Science, Urumqi, China

[5]College of Animal Science and Technology, Sichuan Agricultural University, Chengdu 611130, China

[6]CAAS-ILRI Joint Laboratory on Livestock and Forage Genetic Resources, Institute of Animal Science, Chinese Academy of Agricultural Sciences (CAAS), Beijing, China

[7]Livestock Genetics Program, International Livestock Research Institute (ILRI), Nairobi, Kenya

[8]MOA Key Laboratory of Veterinary Pharmaceutical Development of Ministry of Agriculture (MOA), Lanzhou Institute of Husbandry and Pharmaceutical Sciences of Chinese Academy of Agricultural Sciences, Lanzhou, China

[9]Institute of Animal Science and Veterinary Medicine, Gannan Tibetan Autonomous Prefecture, Hezuo, China

[10]State Key Laboratory of Veterinary Etiological Biology, Lanzhou Veterinary Research Institute, Chinese Academy of Agricultural Sciences, Lanzhou, China

[11]Institute of Animal Husbandry and Veterinary Medicine, Xinjiang Academy of Agricultural and Reclamation Sciences, Shihezi 832000, China

[12]State Key Laboratory of Sheep Genetic Improvement and Healthy Production, Xinjiang Academy of Agricultural and Reclamation Sciences, Shihezi 832000, China

[13]These authors contributed equally: Xin Li, San-Gang He and Wen-Rong Li

*e-mail: menghua.li@cau.edu.cn, xjlmj2006@126.com

Abstract

Understanding the genetic mechanisms of phenotypic variation in hybrids between domestic animals and their wild relatives may aid germplasm innovation. Here, we report the high-quality genome assemblies and high-throughput sequencing of 425 ovine animals, including the Pamir argali (*O. ammon polii*, 2*n* = 56), Tibetan sheep (*O. aries*, 2*n* = 54) and their hybrids (2*n* = 55). We detected genomic synteny between Chromosome 2 of sheep and two acrocentric chromosomes of argali. We revealed consistent satellite repeats around the chromosome breakpoints, which could have resulted in chromosome fusion. We observed many more hybrids with karyotype 2*n* = 54 than with 2*n* = 55, which could be explained by the selfish centromeres, the possibly decreased rate of normal/balanced sperm and the increased incidence of early pregnancy loss in the aneuploid ewes or rams. We identified genes and variants associated with important morphological and production traits (e.g., body weight, cannon circumference, hip height and tail length) that exhibit significant variations. We revealed a strong selective signature at the mutation (c.334C>A, p. G112 W) in *TBXT* and confirmed its association with tail length among sheep populations of wide geographic and genetic origins. We produced an intercross population of 110 F_2 offspring with varied number of vertebrae and validated the causal mutation by whole-genome association analysis. We verified its function using CRISPR-Cas9 genome editing. Our results provide insights into chromosomal speciation and phenotypic evolution and a foundation of genetic variants for the breeding of sheep and other animals.

Key Words: hybrid, genome assembly, whole-genome sequence, chromosomal speciation, phenotypic evolution, morphological and production traits, gene editing, sheep

Introduction

Hybridization is widespread in diverse groups of species across the tree of life (Moran et al. 2021), which results in genomic recombination, mosaics of ancestral segments and phenotypic diversity (e.g., heterosis) and can lead to speciation (Abbott et al. 2013; Goulet et al. 2017; Moran et al. 2021). However, the specific molecular mechanisms underlying these changes remain to be elucidated. Interspecific hybridization between domestic animals and their wild relatives (including the wild ancestors and other wild related species) occurs in several genera (e.g., *Ovis*, *Capra*, *Canis*, *Felis*, *Sus*, *Gallus*, *Anas* and *Camelus*), producing fertile (e.g., domestic animals *versus* wild ancestors) or completely/partially sterile (e.g., domestic animals *versus* some wild relatives except the wild ancestors) progenies with possible phenotypic heterosis and different numbers of chromosomes (Bunch and Foote 1977; Arnold 2004; Randi 2008; Chen 2013; Zhou et al. 2018; Lawal et al. 2020; Luo et al. 2020; Vidale et al. 2022). Thus, the intercross between most domestic animals and their wild relatives other than the wild ancestors provides a useful resource for unveiling the molecular and genetic mechanisms underlying chromosomal, genomic and phenotypic evolution and reproductive isolation (Stelkens and Seehausen 2009; Thomsen et al. 2010; Salviano et al. 2017). Additionally, hybrids also provide a powerful system for dissecting the genetic basis of complex phenotypes in domestic animals (Zhou et al. 2018).

To date, 8 species of the genus *Ovis* have been identified with varying diploid numbers of chromosomes ($2n$ = 52–58), consisting of domestic sheep (*O. aries*) and their seven extant wild relatives (argali *O. ammon*, Asiatic mouflon *O. orientalis*, European mouflon *O. musimon*, urial *O. vignei*, bighorn sheep *O. canadensis*, thinhorn sheep *O. dalli*, and snow sheep *O. nivicola*) (Rezaei et al. 2010; Cao et al. 2021; Chen et al. 2021b). Hybridization between wild relatives, in particular the Pamir argali (also called Marco Polo sheep *O. ammon polii*), which has larger biomass, less sexual dimorphism and the shortest tail of any wild goat-antelope or

sheep (Alexander and David 2005), and domestic sheep has been documented to produce viable and fertile hybrids with significant heterotic effects even though some of them were aneuploid with odd numbers of chromosomes ($2n$ = 55 and $2n$ = 57) (Woronzow et al. 1972; Bunch and Foote 1977; Arnold 2004; Schröder et al. 2016; Alberto et al. 2018). For example, a Chinese native sheep breed, Bashibai, has been developed by intercrossing local sheep with argali in Xinjiang since the beginning of the 20th century (Du 2011). Additionally, genomic tracts of wild introgression have been revealed in domestic sheep, contributing to their adaptive, morphological and production traits (Barbato et al. 2017; Hu et al. 2019; Deng et al. 2020; Cao et al. 2021). Research on the genetic mechanisms and evolutionary dynamics of fertility and heterosis for the hybrids between domestic sheep and their wild relatives has not been explored due to the lack of a chromosome-level reference genome for wild sheep and adequate hybrid samples.

Here, we constructed a large argali-sheep hybrid population (n = 402) and a Texel × Kazakh F_2 intercross population (n =110) with segregation of gene variants and phenotypes (Fig. 1A,B; Supplemental Fig. S1). We produced high-quality chromosome-level genomes of argali, Tibetan sheep and two haplotype-resolved assemblies of the F_1-hybrid. We generated a large set of genomes including populations of the hybrid, the F_2, and sheep with wide geographic origins and variable tail length. We implemented cytogenetic examination, population genomic analyses, genome-wide association studies (GWAS) and genome editing. We mainly aimed at: (*i*) revealing genes and variants for several important morphological and peoduction traits with heterotic effects; and (*ii*) exploring the possible molecular basis underlying the genomic recombination and chromosomal evolution.

Results

Genome assembly and annotation

We assembled three genomes of a Tibetan sheep ewe, an argali ram and a F_1-hybrid ram using a sequencing strategy combining PacBio high-throughput sequencing and Illumina systems (Supplemental Table S1; Supplemental Note 1). The draft and polished assemblies comprise 128 contigs with a contig N50 length of 77.47 Mb for Tibetan sheep and 174 contigs with a contig N50 length of 77.94 Mb for argali (Table 1; Supplemental Note S2). After further scaffolding and clustering using Bionano and Hi-C data, a final genome of Tibetan sheep (2.65 Gb) was *de novo* assembled, consisting of 27 pseudochromosomes with varying sizes from 45.01 Mb to 280.64 Mb, while the *de novo* genome assembly of ram argali had a total length of 2.66 Gb across 29 chromosomes (i.e., 27 autosomes, X Chromosome and Y Chromosome) with variable sizes of 45.10 Mb to 280.78 Mb (Supplemental Fig. S2; Supplemental Table S2). For the F_1-hybrid assay, we first assembled a genome of ~5.21 Gb consisting of 458 contigs with a contig N50 length of 81.34 Mb after correction by the Illumina paired-end data. We obtained 54 clusters of contigs and manually adjusting the Hi-C maps (Supplemental Figs. S3, S4). By performing intragenomic alignment, we preliminarily identified two pseudohaploid genome drafts with 28 (F_1-1) and 26 (F_1-2) pseudochromosomes (Supplemental Fig. S4A). The Hi-C map of F_1-2 showed that cluster LG02 shows false joining compared with LG02 in F_1-1 (Supplemental Fig. S4B,C). After mapping HiFi (high fidelity) reads to LG02 in F_1-2 and further reorienting sequence scaffolds based on read coverage, we successfully divided LG02 into two acrocentric pseudoautosomes. Finally, two high-quality haploid genomes (i.e., 26 autosomes and one X Chromosome from sheep; 27 autosomes and one Y Chromosome from argali) were obtained, with contig and scaffold N50 values of 77.91 Mb and 101.52 Mb for the maternal assembly and 80.50 Mb and 102.90 Mb for the paternal assembly (Table 1; Supplemental Fig. S5; Supplemental Table S2; Supplemental Note S3).

Benchmarking universal single-copy ortholog (BUSCO) analysis showed a high degree of completeness of these genomes containing more than 95% of the complete

eukaryotic universal genes (Supplemental Table S3) (Luo et al. 2020; Yang et al. 2017). The mapping rate and coverage from Illumina reads reached >99%, and each base in the assembly showed a high accuracy of >99.9% (Supplemental Table S3). GC-depth and BLAST analyses did not detect contamination of the genomes (Supplemental Fig. S6; Supplemental Table S3). The distribution of transposable elements (TEs) and tandem repeats (TRs) across the whole genomes showed similarity among them (Supplemental Table S4; Supplemental Figs. S7, S8). The four assemblies showed similar numbers (around 20,000) of annotated protein-coding genes, with an average length of ~47.89 kb for a gene, ~1,645.20 bp for a coding sequence and ~176.88 bp for an exon (Supplemental Table S5). Additionally, we predicted a number of different types of RNA for the four assemblies (Supplemental Table S6).

Genomic characteristics

Of a total of 189,981 protein sequences in sheep, argali and seven other species (i.e., human, dog, horse, pig, cattle, yak and goat), we identified 19,917 gene families (orthogroups) based on homologous proteins. Of these gene families, 14,401 were shared among sheep, argali and goats (Fig. 1D), and a majority of these genes (75.7%–82.1%) within families were single copies across the species (Fig. 1E).

Phylogenetic reconstruction of the 9 mammalian species indicated that argali and Tibetan sheep shared a common ancestor approximately 2.2 (95% CI, 1.9–2.6) million years ago (MYA) based on the 10,043 single-copy orthologous genes (Fig. 1F). Argali showed more events of gene-family contraction (n = 659) and expansion (n = 277) than those of Tibetan sheep (contraction: n =377; expansion: n =255), respectively.

Chromosomal evolution

Cytogenetic analysis showed that the argali's karyotype (2*n* = 56) contains two pairs of metacentric chromosomes and 26 pairs of acrocentric chromosomes, the karyotype of Tibetan sheep (2*n* = 54) consists of three pairs of metacentric chromosomes and 24 pairs of acrocentric chromosomes, and their F_1-hybrid (2*n* = 55) has two pairs of metacentric chromosomes, one unpaired biarmed chromosome, 2 unpaired acrocentric autosomes and 24 pairs of acrocentric chromosomes (Fig. 1C). Of 39 F_1 backcrosses (2*n* = 54/55) with Tibetan sheep (2*n* = 54), we detected 32 individuals with 54 chromosomes and 7 individuals with 55 chromosomes. We did not observe animals with 56 chromosomes (Supplemental Fig. S9; Supplemental Table S7), which could only be generated by two parental individuals with 55 chromosomes, and had previously been reported to occur at a very low proportion (~5.56%; Bunch and Foote 1977).

Chromosomal synteny analysis between argali and domestic sheep showed that pseudochromosomes LG04 and LG07 of argali are syntenic to the long and short arms of Chromosome 2 of domestic sheep, respectively (Fig. 1G; Supplemental Fig. S7A; Supplemental Table S8). Analysis of chromosome collinearity between two subgenomes of the F_1-hybrid also revealed that unpaired biarmed Chromosome 2 of domestic sheep represents a high degree of sequence synteny with two unpaired acrocentric pseudochromosomes LG04 and LG07 of argali (Fig. 1G; Supplemental Fig. S7B; Supplemental Note S4). In the fluorescent in situ hybridization (FISH) analysis, the probes *GNAQ* (guanine nucleotide-binding protein alpha-q; green signal) on the short arm and *STK39* (serine threonine kinase 39; red signal) on the long arm of Chromosome 2 were mapped onto two acrocentric chromosomes of argali (Fig. 1C). We further examined the chromosomal collinearity between goat (*Saanen_v1*, GCA_015443085.1) and ovine species (i.e., Tibetan sheep, argali and the F_1-hybrid). Two biarmed pseudochromosomes (i.e., LG01 and LG02) of argali showed the synteny between the fusions of acrocentric chromosomes 1 and 3 and chromosomes 5 and 11 of goat, respectively. The two biarmed chromosomes have been maintained in

domestic sheep, corresponding to chromosomes 1 and 3. The third biarmed chromosome (i.e., Chromosome 2) observed in domestic sheep was syntenic to the fusion of acrocentric pseudochromosomes LG04 and LG07 in argali, which corresponds to acrocentric chromosomes 2 and 8 of goat (Fig. 1G; Supplemental Table S9).

Robertsonian translocations (ROBs) (e.g., non-allelic homologous recombination, NAHR) involved the breakpoints on chromosomes 1, 3, 2, 8, 5, 11 in goat, pseudochromosomes LG01, 02, 04, 07 in argali and chromosomes 1, 2, 3 in domestic sheep. We found specific repeat sequences in the regions adjacent to the centromeres of these three species (Fig. 2A). For ROB(G1qG3q) and ROB(G5qG11q) of goat, the common specific repeats of ROB(G1qG3q) (i.e., CGTGGGAAAGCCT) and ROB(G5qG11q) (i.e., GTGGGAAAGCCTC) occurred 3–4 times on chromosomes 3 and 5 but were repeated many more times (79–476) on chromosomes 1 and 11. A large number (968–1,786) of repeat sequences, "GGGGGCCCACGTGATTG(T)CCCCT", were located on chromosomes 3 and 5 but not on chromosomes 1 or 11. For ROB(G8qG2q), the sequences "GGGGGCCCACGTGATTG(T)CCCCT" and "TTTCCCACGAGGC" were repeated several hundreds of times (13–469) on chromosomes 2 and 8 of goat, but they were lost, and only the repeat "TTTCCCACGAGGC" was retained in argali and domestic sheep (Fig. 2A; Supplemental Fig. S10; Supplemental Table S10). This observation indicated that the sequence-specific recognition between homologous DNA elements on nonhomologous acrocentric chromosomes could be the underlying molecular basis of such chromosome fusions in ovine species. During the backcrossing between the F_1-hybrid and domestic sheep, a high sequence similarity between the meta-centric chromosome and two acro-centric autosomes could account for the successful homologous chromosome pairing during meiosis, mainly giving rise to normal/balanced embryos after fertilization with the normal gametes of domestic sheep (Fig. 2B).

Pattern of variations and genetic differentiation

Whole-genome sequences of 425 individuals (i.e., 89 Tibetan sheep, 8 argali and 328 hybrids) (Fig. 1B) showed an average depth of ~17.88× and a genome coverage of 99.29% (Supplemental Table S11). After variant calling and filtering, we obtained a total of 31.86 million SNPs, including 17.59 million SNPs (14.71–14.99 million per individual) in argali, 31.86 million SNPs (12.00–18.82 million per individual) in the hybrids and 26.64 million (10.29–12.15 million per individual) in Tibetan sheep (Supplemental Fig. S11A,B; Supplemental Table S12). In addition, we observed 5.34 million indels (0.88–1.60 million per individual) (Supplemental Table S12).

Principal component analysis (PCA) and clustering analyses based on maximum likelihood estimation separated the samples into three separate clusters, argali, Tibetan sheep and their hybrids (Fig. 3A,C). Genomic diversity (π) based on SNPs was 1.13×10^{-3} for argali, 3.11×10^{-3} for Tibetan sheep and 3.78×10^{-3} for the hybrids (Fig. 3B). Pairwise genome-wide F_{ST} values calculated by SNPs were 0.38 between argali and Tibetan sheep, 0.26 between argali and the hybrids and 0.03 between Tibetan sheep and the hybrids.

GWAS of morphological and production traits

In general, argali have a larger body size and shorter tail than those of Tibetan sheep (Alexander and David 2005). In Tibetan sheep and the hybrids, the Pearson correlation coefficient for morphological and production traits such as body weight, body height, body slanting length, chest circumference, cannon circumference and hip height showed a strong (r^2 = 0.6–0.8) and significant ($P < 0.05$) correlation between them (Supplemental Table S13). The hybrids showed significant heterosis over Tibetan sheep for traits such as body weight and body height (Supplemental Fig. S12). In the backcross/intercross hybrid population, GWAS analysis revealed multiple quantitative trait loci (QTLs) for body weight, body height, body slanting length,

chest circumference, cannon circumference, hip height, hip width and tail length, respectively (Supplemental Table S16). Within each set of significant SNPs, we estimated the levels of LD (r^2) among the loci on each chromosome. At the LD threshold value of $r^2 = 0.6$ and an interval distance ≥ 1Mb, we concluded that the significant SNPs represent 13, 5, 4, 5, 7, 6, 1 and 1 independent QTLs for body weight, body height, body slanting length, chest circumference, cannon circumference, hip height, hip width and tail length, respectively (Supplemental Figs. S13–S15; Supplemental Tables S16, S17; Supplemental Note S5). Through examining the independent QTLs for each trait on each chromosome (Supplemental Figs. S14 and S15), we found that the QTLs (Chr.2: 90,071,756-98,428,523 bp, Chr.6: 28,993,028-30,457,109 bp, Chr.7: 11,574,342-14,364,056 bp) for body weight, the QTLs (Chr.7: 11,757,199-14,356,384 bp) for body height, the QTLs (Chr.2: 96,177,779-98,428,159 bp, Chr.6: 28,993,028-30,401,993 bp) for body slanting length, the QTLs (Chr.7: 11,595,855-14,356,384 bp) for cannon circumference and the QTLs (Chr.7: 11,563,650-14,461,622 bp) for chest circumference have overlapping and broad signals, which could be due to structural variants (e.g., an inversion). Further annotation of the significant GWAS signals in their upstream and downstream genomic regions revealed a number of genes associated with these morphological and production traits (Supplemental Table S18). Within these functional genes, we calculated the r^2 between the top signals with the other signals, and selected those independent loci under the LD criteria of $r^2 < 0.6$ and an interval distance ≥ 1Mb, such as *TEK* (Chr.2: 96,177,779), *FLRT2* (Chr.7: 96,426,040), *IQCH* (Chr.7: 14,356,384), *AUTS2*, *CASTOR2* (Chr.24: 35,060,092) for body weight, *MSRA* (Chr.2: 104,441,386), *IQCH* (Chr.7: 14,356,384), *UBASH3B* (Chr.15: 33,383,374) for body height, *TEK* (Chr.2: 96,177,779), *LINGO2* (Chr.2: 98,428,159), *BMRP1B*, *PDLIM5* (Chr.6: 30,401,933), *IQCH* (Chr.7: 14,356,384) for body slanting length, *PCDH10*, *HMGN1* (Chr.17: 26,391,533) for chest circumference, *LGALSL* (Chr.3: 44,121,028), *IQCH* (Chr.7: 14,356,384), *TFB2M* (Chr.12: 30,675,722) for cannon circumference, *MRS2* (Chr.20: 32,952,100) for hip height, and *ACTR3B*, *DPP6* (Chr.4:

117,196,289) for hip width (Supplemental Table S18; Supplemental Fig. S16). Of the genes identified here, several (e.g., *PCDH10*, *HMGN*, *TEK*, *BMPR1B* and *IQCH*) were associated with two or more of the morphological and production traits (Supplemental Table S16), probably due to strong genetic correlations between the traits (Sieber et al. 1988). Overall, the genes play important roles in obesity, regulation of feeding, spine morphogenesis, bone formation and skeletal muscle development (Supplemental Table S18).

In particular, we detected 43 significant SNPs in and between the *PCDH10* and *HMGN1* genes associated with body weight traits. *PCDH10* has been reported to be associated with carcass weight and bone weight in cattle (Wang et al. 2018b). *HMGN1* functions in promoting astrocyte differentiation and regulating feeding (Hsuchou et al. 2009; Nagao et al. 2014; Xu and Xie 2016) (Fig. 4D). These signals showed strong LD with the most significant SNP (Fig. 4E), and the phenotypic data of body weight associated with the three genotypes (TT, TG and GG) of the top SNP (Chr. 17: 26,391,397) showed a significant (Mann–Whitney *U* test, $P < 0.001$) difference between each other (Fig. 4F). For tail length, we identified a single contiguous genomic region on Chromosome 8 (Chr. 8: 88.34 Mb to 88.43 Mb), including two of the most significant signals located in the *TBXT* gene (Fig. 4A,B; Supplemental Note S5). *TBXT* is known as a founding member of the T-box transcription factor family and is expressed only in the early stages of notochord development, reportedly affecting tail length and sacral vertebrae in heterozygous animals by regulating the transforming growth factor and Wnt signaling pathway during vertebrae development (Supplemental Fig. S17A) (Smith et al. 1991; Martin and Kimelman 2008; Han et al. 2019). The two top linked signals in *TBXT* contain one missense transversion mutation (Chr8: 88,341,610 C/A), c.334C>A (CCC>ACC), leading to the conversion of glycine to tryptophan. Phenotypic data indicated that individuals with the homozygous reference genotype (CC) had a significantly (Mann-Whitney *U* test, $P < 0.001$) longer tail length than individuals with the

heterozygous variant genotype (CA), while individuals with the homozygous variant genotype (AA), which showed specific geographic and genetic origins (see below), were not observed (Fig. 4C).

Selective and association signatures associated with tail length and validation of the *TBXT* gene

We focused on the tail length trait from a wide range of origins. We integrated the whole genomes of 189 sheep (~8.96×) from ten domestic populations (Cheng et al. 2022; Pan et al. 2018; Wang et al. 2018a) with variable tail length. Compared with fat-tailed sheep, fat-rumped sheep showed shorter tails (Fig. 5A,B). In the genome-wide scans for selective signatures between 103 fat-rumped sheep (i.e., 28 Kazakh sheep, 19 Bashibai sheep, 30 Bayinbuluke sheep and 26 Duolang sheep) and 86 fat-tailed sheep (i.e., 30 Cele Black sheep, nine Hetian sheep, ten Hu sheep, ten Wuzhumuqin sheep, nine Small-tailed Han Sheep and 18 Tan sheep) (Supplemental Table S19), we identified 168 and 211 candidate selected regions (top 0.5% outliers) by the F_{ST} and π ratio methods, respectively. The strongest signal was located on Chromosome 8, ranging from 87.56 to 87.88 Mb (Fig. 5C; Supplemental Table S20). In this candidate selective region, we further estimated genetic differentiation at the individual SNP level by estimating the π and Tajima's D values between fat-rumped and fat-tailed populations. We observed the two most significantly differentiated SNPs (c.333C>G and c.334C>A) in the *TBXT* gene (Fig. 5D). Moreover, we genotyped the nonsynonymous SNP (c.334C>A, p. G112 W) in *TBXT* in 867 sheep representing 19 populations from a worldwide origin. We found that mutant allele A occurred at high frequency in fat-rumped sheep, whereas the wild allele C appeared with high frequency in fat-tailed and thin-tailed sheep (Supplemental Table S21). In addition, we generated a Texel (thin-tailed with more vertebrae) × Kazakh (fat-rumpled with fewer vertebrae) F_2 intercross population of 110 sheep (Supplemental Fig. S1; Supplemental Table S22) and performed GWAS analysis of the traits of tail length and number of caudal vertebrae (Fig. 5F). Both the

nonsynonymous SNP c.334C>A and the synonymous SNP c.333C>G in the *TBXT* gene showed the highest significance for the two traits (Supplemental Table S23). At the SNP c.334C>A, the F_2 offspring with the AA genotype showed the tailless phenotype, while offspring with the CC genotype had thin and long tails (Fig. 5G,H). Both genotypes showed significant (Mann-Whitney *U* test, $P < 0.001$) differences between tailed and tailless sheep in the F_2 intercross population. Thus, our data of the worldwide populations and the F2 intercross confirmed the previously reported association between the two mutations in *TBXT* and the number of caudal vertebrae (Han et al. 2019).

We validated the phenotypic effect of the C334A mutation in sheep by CRISPR-Cas9 (Fig. 5I). After microinjection, 338 injected embryos were transplanted into 216 surrogate ewes of Chinese Merino sheep. Finally, 31 surrogate ewes successfully produced 28 offspring. By screening the mutation in lambs, we identified 19 mosaic merino mutants, including 13 sheep with the C334A target mutation (TM), five sheep with a short indel (KO) and one sheep (ID: GM079) with both the target mutation and an 8-bp deletion (Fig. 5J). The sheep GM079 had the shortest tail with a tail length of 10 cm and 11 caudal vertebrae compared with wild-type merino sheep, with an average tail length of ~25.71 cm and caudal vertebrae length of ~18.47 (Fig. 5K; Supplemental Table S24). The average tail length and number of caudal vertebrae for the KO (tail length: 19.33 cm; number of caudal vertebrae: 15.17) and TM (tail length: 20.82 cm; number of caudal vertebrae: 15.07) merino animals were significantly shorter/lower than those for the wild-type merino sheep (tail length: 25.71 cm; number of caudal vertebrae: 18.47) (Mann–Whitney *U* test, $P < 0.05$) (Fig. 5M; Supplemental Table S24). Additionally, we crossed the individual GM079 with normal Merino sheep and generated 19 heterozygous progenies for the SNP mutation C334A and five heterozygous progenies for the 8-bp deletion. The number of caudal vertebrae trait showed a significant difference between these heterozygous progenies

and wild-type merino sheep (Mann-Whitney *U* test, $P < 0.001$) (Fig. 5L,5N; Supplemental Table S25).

Discussion

Robertsonian translocation occurs in a few mammals, such as humans (Page et al. 1996), dogs (Mayr et al. 1986) and water buffaloes (Luo et al. 2020). In humans, it involves five acrocentric chromosomes, 13, 14, 15, 21 and 22, all of which have very small short arms containing no unique genes (Song et al. 2016). Recombination between homologous sequences on nonhomologous chromosomes, which leads to the preferential formation of rob(13q14q) and rob(14q21q), has been proposed as the primary reason for this translocation in humans (Page et al. 1996). In the *Ovis* genus ($2n$ = 52–58), previous cytogenetic analysis revealed four chromosomal fusions from the metacentric chromosomes of goats, corresponding to centric fusions of goat ($2n$ = 60), namely, chromosomes 1/3, 2/8, 5/11 and 9/19 sequentially (Bunch et al. 2006). However, we observed that the second pair of metacentric chromosomes in argali ($2n$ = 56) is the result of the fusion of chromosomes 5 and 11 of goat, while chromosomes 2 and 8 from goat fused to give rise to the third pair of metacentric chromosomes of domestic sheep ($2n$ = 54).

Of 39 F_1 backcrosses ($2n$ = 54/55) with Tibetan sheep ($2n$ = 54), we observed a much higher frequency of animals with 54 (number of animals = 32, 82.05%) chromosomes than with 55 chromosomes (number of animals = 7, 17.95%). This observation suggested that the descendants inclined to generate a more stable karyotype with 27 pairs of chromosomes but not 26 pairs of chromosomes together with one unpaired biarmed autosome and 2 unpaired acrocentric autosomes (Bunch and Foote 1977). Notably, we found that Chromosome 2 of domestic sheep contains more satellite repeats (175 repeats) than the other two acrocentric chromosomes (LG04 and LG07) of argali (19 and 33 repeats, respectively) (Fig. 2A), which may make Chromosome 2 more “selfish” to assemble a larger kinetochore and have a higher chance of facing

410 the “egg side” during the first meiotic division of the F_1-hybrid oocyte ($2n = 55$) (Fig.
411 2C) (Nikalayevich and Verlhac 2021). Previous studies reported that when “selfish”
412 chromosomes face the polar body side and sense the proximity of the cortex, they will
413 dissociate the attachment to the spindle, which makes it possible for them to reorient
414 and reattach until they face the egg side (Fig. 2C) (Akera et al. 2017; Akera et al.
415 2019). Thus, this genetic mechanism may explain the priority of generating gametes
416 with 27 chromosomes over 28 chromosomes for the F_1 hybrids ($2n =55$), which could
417 have contributed to the chromosomal speciation.
418
419 In humans, 99.7 % of sperm from the homozygous Robertsonian translocation carrier
420 (44, XY) were normal/balanced, which is much higher than that (79.9%) from the
421 heterozygous Robertsonian translocation carrier (45, XY) (Song et al. 2016). Most
422 conceptuses with autosomal aneuploid perish *in utero*, which makes aneuploidy the
423 leading genetic cause of early pregnancy loss (Hassold and Hunt 2001; Kurahashi et
424 al. 2012). Therefore, the possibly decreased rate of normal/balanced sperm and
425 increased incidence of early pregnancy loss in aneuploid ewes or rams ($2n = 55$) could
426 also account for many more hybrids with $2n = 54$ than with $2n = 55$ observed here.
427
428 We have generated high-quality assemblies of Tibetan sheep, argali and the F_1-hybrid,
429 which have provided important insights into the molecular mechanisms of
430 chromosomal fission/fusion among ovine species. Additionally, the assemblies can be
431 integrated with those of other species to fully exploit the genome divergence and
432 chromosomal evolution among species of the Ovis genus and the subfamily Caprinae.
433 Since the assemblies are among only few high-quality chromosome-level reference
434 genomes of high-altitude vertebrates (but see yak (*BosGru3.0*, GCA_005887515.2)),
435 they will be of great importance in exploring the genetic mechanisms underlying
436 high-altitude genetic adaptation. Moreover, understanding the molecular basis of
437 heterosis and phenotypic variation requires knowledge of diploid alleles (Sun et al.
438 2020). The high-resolution species-specific haploids of the F_1-hybrid can provide the

diploid chromatin architecture for understanding the parent-of-origin effects and the regulation (e.g., *cis*- or *trans*-acting regulatory variation) of allele-specific expression (ASE) between homologous chromosomes. Additionally, haplotype-resolved diploid genomes of the F_1-hybrid will help to elucidate the landscape of genome rearrangements (SVs, indels and TEs) and the epigenetic regulation of haploid-specific gene expression during hybridization, which could account for heterosis and ASE (McClintock 1984; Han et al. 2020). Assemblies of interspecies F_1 hybrid diploid genomes have been reported in cultured fish (S. asotus; $2n = 58$) × (S. meridionalis; $2n = 58$) (Chen et al. 2021a), yak (*B. grunniens*; $2n = 60$) × cattle (*B. taurus*; $2n = 60$) (Rice et al. 2020) and domestic cat (*F. catus*; $2n = 38$) × Asian leopard cat (*P. bengalensis*; $2n = 38$) (Bredemeyer et al. 2021). However, representative assemblies of aneuploidy ($2n = 55$) with odd numbers of chromosomes have rarely been reported, but these resources would aid in dissecting the genetic basis of reduced fertility, interspecific hybridization compatibility and speciation (Pauciullo et al. 2016; de Vos et al. 2020).

Body weight, body height, body slanting length, cannon circumference, chest circumference, hip height, hip width and tail length are important morphological and production traits that remain the main selective targets of current livestock breeding programs. Our results unraveled many previously unreported trait-associated genes and variants as well as those with reported functions (e.g., *PTPRG*, *CACNB2*, *GALNTL6* and *TMEM132D*). A majority of these quantitative traits such as body weight and body height are complex and multigenic traits (Yang et al. 2011b), which, however, are difficult to modulate with genome editing (Blighe et al. 2018).Tails are a vital part of the evolutionary package and play important roles in many mammals, such as counterbalancing (e.g., cats and kangaroos) (Walker et al. 1998; O'Connor et al. 2014), defense (porcupine) (Mori et al. 2014), warning signals (e.g., danger in deer) (Caro et al. 1995), social and emotional signals (canids;) (Siniscalchi et al. 2013), hunting (alligator) (Willey et al. 2004) and fly swatting behavior in livestock such as

cows, horses and sheep. The prehensile tails of some mammals (e.g., monkeys) are used to increase mobility and stability (Young et al. 2015). Tails on sheep lambs are typically docked in most breeds for health reasons (Smith et al. 1997). Nevertheless, docking is not necessary in short-tailed breeds, and tails are not usually docked in breeds in which a long tail is valued, such as the Zwartbles breed with white socks and white tips on their tails (Lauvergne and Hoogschagen 1978). Docking is often considered cruel and unnatural by animal welfare activists, but it is considered essential in maintaining the health of sheep by sheep farmers (Brown and Meadowcroft 1996; Weaver 2005). Additionally, long and wooly tails in sheep make shearing more difficult, interfere with mating, and make the animals extremely susceptible to parasites, especially those that cause flystrike (Wooster 2005). These genes and alleles, along with the identified new genes and variants, provide useful resources for understanding the genetic basis of various phenotypic traits.

Early studies showed that individuals with homozygous *TBXT* mutations always exhibit severe developmental disorders (Meisler 1997), and even specific amino acid changes are lethal in the early fetal life of animals (e.g., mouse, cat and dog) (Haworth et al. 2001; Wu et al. 2010; Buckingham et al. 2013). However, the fat-rumped sheep population and intercross population with homozygous AA at nt 334 of exon 2 of *TBXT* showed no cases of lethality or other birth defects (Fig. 5E). A very recent study reported that the simian-specific *Alu*Sx1 element and hominoid-specific *Alu*Y element in the *TBXT* gene can form an inverted repeat pair, leading to an alternative splicing isoform without exon 6 for the *TBXT* gene and further causing reduction or loss of an external tail in hominoids (Xia et al. 2021). In mice, deletion of exon 6 in the *TBXT* gene could induce tail loss (Xia et al. 2021). In humans, the rs2305089 polymorphism in the *TBXT* gene and the epigenetic inactivation of *TBXT* by H3K27 were reported to be associated with chordoma (Cottone et al. 2018; Jalessi et al. 2022). The missense mutation (c. G47T, p. R16L) in *TBXT* is related to the development of congenital scoliosis (Feng et al. 2021). This

and a previous study suggested different genetic mechanisms for vertebrae variation in mammals (Supplemental Fig. S17B). Therefore, analysis of the origins of these genes and variants will provide new insights into the evolution of trait-associated alleles during domestication and artificial selection. We detected a few trait-associated genes/variants that were nearly fixed in wild introgressive regions in the hybrids. This distinct feature suggests that introgression of new genes/alleles from their wild relatives might be a hallmark of livestock breeding through hybridization. In addition, our results indicated that introgression from wild relatives is a very important source of new genetic variation when adapting to a new environment (Wu et al. 2018; Mabry et al. 2021). Our results suggest that these species do not evolve in genetic isolation and point out future directions in the germplasm collection and utilization of wild relatives, which could broaden the genomic diversity of domestic animals (Zhou et al. 2018).

In conclusion, we have generated high-quality complete assemblies for argali, Tibetan sheep and their F_1-hybrid with two sets of different haploid chromosomes as well as high-depth WGS of the interspecific hybrids, intercross population and native sheep breeds. We demonstrate a case for creating new traits in domestic animals on a short timescale by combining the desirable attributes of wild relatives. Genomic recombination may help to maintain a repository of epigenes or epialleles generated by interspecific hybridization and intercrossing. The resources generated here provide a genomic framework for future germplasm use and expedite breeding and genetic improvement of sheep and possibly other livestock.

Material and Methods

Sampling and DNA extraction

Genome assembly. A blood sample was collected from a Tibetan sheep ewe (*Ovis aries*, $2n = 54$), and fibroblasts were collected from the skin of a wild Marco Polo ram

(a subspecies of argali *Ovis ammon polii*, 2*n* = 56) and an F_1-hybrid ram of Marco Polo sheep and Tibetan sheep (*Ovis ammon polii* × *Ovis aries*; 2*n* = 55) for genome assembly. Tibetan sheep were ethically sacrificed, and various tissues, such as heart, liver, spleen, lung, skeletal muscle, esophagus, uterus, trachea, small intestine and skin tissues, were snap frozen in liquid nitrogen and stored at -80 °C until further use. The fibroblasts were cultured in DMEM (GIBCO, USA) supplemented with 10% FBS (GIBCO) and 1% antibiotic-antimycotic (GIBCO) at 37 °C under 5% CO_2.

Population genomics analysis and whole-genome association study (GWAS). For the whole-genome association study (GWAS) analysis of morphological and production traits, a total of 402 blood samples were collected, including 74 Tibetan sheep and 328 hybrid descendants of Tibetan sheep and the Marco Polo subspecies of argali produced in 5 generations and more than 10 years. In addition to the whole-genome sequences generated here, genomes of 15 Tibetan sheep and 8 argali from our previous studies (Deng et al. 2020; Cao et al. 2021; Lv et al. 2022) were integrated in the population genomics analyses, totaling 425 genomes with an average depth of 17.88×. Furthermore, we produced an intercross population between Texel (thin-tailed with more vertebrae) and Kazakh (fat-rumpled with fewer vertebrae) sheep, consisting of 110 F_2 offspring (average depth = 10.98 ×). We created the F_1 population by mating four Texel rams with 220 Kazakh ewes. Of the F_1 population, four rams were mated with 116 ewes, producing the F_2 population of 110 offspring with varied numbers of vertebrae. We measured the tail length and number of vertebrae via CT scanning and included them in the GWAS analysis of the two traits.

Whole-genome selection test. A total of 189 publicly available genomes from ten domestic populations were integrated in the selection tests related to the tail-length trait, with a mean coverage of 8.96 × (Supplemental Methods; Supplemental Table S19).

Genome and transcriptome sequencing

After SMRT sequencing libraries construction, DNA fragments selection and purification, for Tibetan sheep and argali, sequencing were performed on a PacBio Sequel II instrument using continuous long-read sequencing (CLR) mode, while for the F_1-hybrid sample, sequencing was performed on a PacBio Sequel II instrument using circular consensus sequencing (CCS/HiFi) mode (Supplemental Methods). Finally, three SMRT cells for Tibetan sheep, two cells for argali and five cells for the F_1-hybrid were used to generate raw data, respectively. Raw sequencing data were processed to remove low-quality reads and adapters using the PacBio SMRTlink v8.0 pipeline.

For genome assembly, libraries for Illumina sequencing were prepared using TruSeq PCR-free preparation kits (Illumina, San Diego, CA) with an insert size of ~ 350 bp and sequenced on the Illumina NovaSeq/MGI-2000 platform. For whole-genome resequencing, paired-end sequencing libraries were constructed and sequenced on the Illumina HiSeq X Ten platform. After mapping 150-bp paired-end reads onto the assembly genomes of domestic sheep using the BWA-MEM v.0.7.17 (Li and Durbin 2009), SNP calling was performed using HaplotypeCaller in GATK (McKenna et al. 2010) for each individual (Supplemental Methods).

After RNA extraction, measurement of the concentration and integrity, and library construction, RNA sequencing were performed on Illumina NovaSeq/MGI-2000 platform and PacBio Sequel II machine, respectively (Supplemental Methods).

Genome assembly and scaffolding

For Tibetan sheep and argali, we used NextDenovo v2.3.1 (https://github.com/Nextomics/NextDenovo) to generate the draft assembly. For the F_1-hybrid, the software hifisam v0.12 (Cheng et al. 2021) was used for the preliminary assembly, and NextPolish (Hu et al. 2020) was then used to polish all

assemblies (Supplemental Methods). After evaluation of the draft assemblies (Supplemental Methods), we generated optical maps. DNA molecules were recorded in the Bionano Genomics Saphyr system (Supplemental Methods). Contigs were assembled into scaffolds using the Hybrid Scaffolding pipeline of the Bionano Solve v3.3 package (Mostovoy et al. 2016).

To further order and orient sequence scaffolds along chromosomes, we used genome-wide chromatin interaction data (Hi-C reads) sequenced by the Illumina NovaSeq/MGI-2000 platform. After filtering, valid interactive paired reads were identified and retained by HiC-Pro v2.8.1 (Servant et al. 2015) (Supplemental Methods). We then used the LACHESIS software package (https://github.com/shendurelab/LACHESIS) (Burton et al. 2013) to cluster, order, and orient scaffolds on chromosomes (Supplemental Methods). Finally, placement and orientation errors exhibiting obvious discrete chromatin interaction patterns were manually adjusted.

To generate two pseudohaploid genome drafts of the F_1-hybrid, we retained the chromosomes with an overlapping region and manually copied this region to the corresponding position of the homologous chromosome based on the Hi-C maps of the normalized contact matrix for the overlapping regions in homologous chromosomes (Supplemental Fig. S3). We then identified homologous chromosomes by performing intragenomic alignment and aligning the two pseudohaploid assemblies to the argali and Tibetan sheep genome assemblies using the NUCmer program in MUMmer v.4.0.0 (Marçais et al. 2018). To divide the LG02 cluster in one of the pseudohaploid genome drafts (F_1-2) into two acrocentric pseudochromosomes, we mapped HiFi reads back to F_1-2 using minimap2 (Li 2018) and calculated the mapping depth and coverage for each base on LG02 through SAMtools v1.4 (Li et al. 2009). We then reordered and reoriented sequence scaffolds of LG02 using Hi-C data based on the coverage. Finally, we redefined two highly resolved pseudohaploid

genome drafts as species-specific haploids based on the coverage rate between two homologous chromosomes and their parental assemblies (i.e., argali and Tibetan sheep). For the homologous chromosomes (i.e., LG09 in F_1-1 and LG11 in F_1-2) that failed to be assigned, we used the argali-specific SNPs inferred from the 425 argali and domestic sheep whole-genome data as markers to define species-specific chromosomes.

Genome annotation

*Repeat prediction and noncoding RNA annotation***.** We used GMATA v2.2 (Wang and Wang 2016) and Tandem Repeats Finder v4.07b (Benson 1999) to search for tandem repeats in the assembled genomes. RepeatMasker v r1.331(Bedell et al. 2000) was applied to search for TEs. To obtain a reliable profile of noncoding RNA, we aligned the assembly against the Rfam database (Griffiths-Jones et al. 2005) using the program cmscan in the software Infernal v1.1.2 (Nawrocki and Eddy 2013). Furthermore, we used tRNAscan-SE v2.0 (Lowe and Eddy 1997) and RNAmmer v1.2 (Lagesen et al. 2007) for tRNA and rRNA predictions, respectively.

*Gene annotation***.** The gene models generated from the following three approaches were integrated with EvidenceModeller v1.1.1 (Haas et al. 2008) (Supplemental Methods): (*i*) For annotation using RNA-seq, we combined transcripts generated from Illumina RNA-seq and PacBio Iso-Seq to predict open reading frames (ORFs) using PASA v2.3.3 (Haas et al. 2008). (*ii*) For *de novo* gene prediction, AUGUSTUS v3.3.1 (Stanke et al. 2008) was applied to predict genes using a generalized hidden Markov model (GHMM) (Stanke et al. 2006). (*iii*) For the homology-based prediction, it was implemented by aligning the protein sequences of other species to the assembled genome using GeMaMo v1.6.1 (Keilwagen et al. 2016). Finally, we integrated these three predicted gene sets based on the relative weights (10:1:5) for transcriptomic, *de novo*, and protein homology-based evidence using EvidenceModeller v1.1.1. The genes with TEs were removed by TransposonPSI (Urasaki et al. 2017), and the

miscoded genes were further filtered. Functional annotation of the predicted genes was obtained by aligning the protein sequences of these genes against the sequences in the NCBI nonredundant protein database and four public protein databases (Supplemental Methods). All the gene symbols were named according to the nomenclature guidelines from the Human Genome Organisation (HUGO) Gene Nomenclature Committee (https://www.genenames.org).

Comparative analysis of genome assemblies

To analyze the chromosomal collinearity between species, we first aligned all the assemblies of species using the NUCmer program in the MUMmer v.4.0.0 package (Marçais et al. 2018). The positions of syntenic and rearranged regions and local sequence variations in the regions were mapped using the show-snps program in MUMmer and Assemblytics software v1.2.1 (Nattestad and Schatz 2016). Alignment coordinates were then extracted using show-coords in MUMmer with the -THrd option, and chromosomal features and synteny of the assemblies were plotted using Circos (Krzywinski et al. 2009). Tandem repeats in the region surrounding the breakpoints were identified by TRF software (Benson 1999). In addition, we plotted macrosynteny for the genome assemblies of goat Saanen_v1 (GCA_015443085.1), argali (JAKZEL000000000), Tibetan sheep CAU_O.aries_1.0 (GCA_017524585.1) and the F_1-hybrid (JALAIW000000000 and JALAIX000000000) using MCscan (Python version) (Wang et al. 2012).

To identify the number of gene families and number of gene copies in specific families, annotated genomic information for various species were retrieved (Supplemental Methods). Classification of all the annotated protein-coding sequences into gene families was performed using OrthoFinder (Emms and Kelly 2019). Phylogenetic trees were built by IQ-TREE (Minh et al. 2020) with 1000 bootstrap replicates. The divergence time was estimated with PAML MCMCTree (Yang 2007) based on the JC69 model, and the nodes were calibrated using five reported

divergence times: 1.94–2.61 MYA for *O. aries* and *O. ammon polii* (Yang et al. 2017), 2.9–7.6 MYA for *B. taurus* and *B. grunniens* (Luo et al. 2020), 18–22 MYA for *Bovinae* and *Caprinae*, 48.3–53.5 MYA for *Ruminantia* and *Suina* and 95.3–113 MYA for *Euarchontoglires* and *Laurasiatheria* (Benton and Donoghue 2007). We then applied the CAFE v4.2.1 program (Han et al. 2013) to examine the expanded and contracted gene families along different nodes of a given phylogeny.

Cell cultures and karyotyping

For argali and the F_1-hybrid assays, chromosome preparations were made from a fibroblast culture mix composed of 10 ml of DMEM with L-glutamine, fetal calf serum (10%), and a penicillin–streptomycin mixture (1%). For Tibetan sheep and the 68 hybrid descendants, whole blood samples were collected from the jugular vein, and chromosome preparations were made from a leukocyte culture mix composed of 7 ml of RPMI medium with L-glutamine, fetal calf serum (20%), penicillin–streptomycin mixture (1%) and concanavalin A with a final concentration of 5 μg/ml. After incubation at 37.5 °C for 45 h, cell cultures were subjected to colchicine (0.07 μg/ml) treatment for 5 h. Following centrifugation, the cells were swollen in hypotonic 75 mM KCl saline solution and fixed in fixative (methanol: glacial acetic acid = 3:1) (Iannuzzi and Di Berardino 2008). Cell suspensions were dropped onto clean and wet slides and then air dried. After Giemsa staining, the slides were observed under a Leica DM6B microscope equipped with a camera.

Probe production and fluorescent *in situ* hybridization (FISH)

Two chromosome painting probes for the *STK39* gene (on the long arm) and *GANQ* gene (on the short arm) located on metacentric Chromosome 2 of the Tibetan sheep assembly were produced by PCR and labeled with TexasRed-dUTP and FITC-dUTP through nick translation. The information for the PCR primers and the length of amplified DNA fragment were detailed in Supplemental Table S26. In FISH, metaphase spreads were first permeabilized using Triton X-100 for 10 min and rinsed

699 in PBS for 5 min, then treated with pepsin at room temperature for 5 min, rinsed in
700 PBS for 5 min twice, and in 70% ethanol for 30 s. After the slides were air dried and
701 dehydrated with a gradient of 70%, 85% and 100% of cold ethanol for 2 min,
702 respectively, a 10-μl probe solution was used for each slide and then denaturing was
703 performed for 2 min at 72–73 °C. The hybridization was performed in a humid
704 chamber at 37 °C for at least 16 h. After hybridization, the slides were washed in 0.3%
705 Igepal, CA-630, Sigma (or NP40)/0.4XSSC at 73 °C for 2 min and then washed in 0.1%
706 IgEpal CA-630, Sigma (or NP40)/2XSSC at room temperature for 90 s. Finally, slides
707 were counterstained with DAPI (4', 6-diamidino-2-phenylindole) solution (0.24 μg/ml,
708 Sigma-Aldrich), and the images were captured with an Olympus BX-51 microscope
709 equipped with a DP-70 CCD camera.
710
711 **Population genomics analysis**
712 In population genomics analyses, SNPs and SVs that did not meet one of the
713 following criteria were excluded: (*i*) a minor allele frequency >0.05; and (*ii*)
714 maximum missing rate <0.1. Principal component analysis (PCA) of whole-genome
715 SNPs and SVs for all 425 individuals was performed with GCTA v.1.24.2 (Yang et al.
716 2011). Population structure was examined using ADMIXTURE v.1.23 with the
717 default settings (Alexander et al. 2009). The number of assumed genetic clusters, *K*,
718 was set as 2. An individual-based neighbor-joining (NJ) tree was constructed for all
719 the samples based on the nucleotide p-distance matrix using TreeBeST v 1.9.2
720 (Vilella et al. 2009) and visualized using FigTree v.1.4.4
721 (http://tree.bio.ed.ac.uk/software/figtree/). The parameter r^2 for LD was calculated for
722 pairwise SNPs within each chromosome using PLINK v.1.90 (Purcell et al. 2007).
723 Nucleotide diversity (π) and pairwise genome-wide F_{ST} values were calculated using
724 VCFtools v.0.1.16 (Danecek et al. 2011).
725
726 **GWAS analysis of morphological and production traits**

Genome-wide association analyses of phenotypic traits such as body weight, body height, body slanting length, cannon circumference, chest circumference, hip height, hip width, and tail length were performed in a total of 402 animals (74 Tibetan sheep and 328 Tibetan sheep × argali hybrid descendants) (Supplemental Table S14) using the EMMAX (efficient mixed-model association expedited) statistical test approach (Kang et al. 2010), which is based on a mixed linear model and accounts for population stratification and relatedness (Supplemental Note S6). To estimate the effect of age on phenotypic data, we implemented analysis of variance (ANOVA) and selected various sets of samples for each different trait in GWAS analysis based on Duncan's multiple range test (Supplemental Table S15). The covariates used to adjust for each phenotype simultaneously are also listed in Supplemental Table S15. For body weight, body slanting length and tail length, the genome-wide significance thresholds were set as $-\log_{10}(0.05/\text{Total SNPs}) = 8.88$ after the Bonferroni correction. We set the thresholds as $-\log_{10}(P\text{-value}) = 8$ for body height and $-\log_{10}(P\text{-value}) = 7$ for cannon circumference, chest circumference, hip height, hip width (Xiao et al. 2021).

Selection test, GWAS and functional validation of *TBXT*

Genome-wide selection tests for the tail length trait. we implemented selective sweep tests between the genomes of 103 fat-rumped sheep and 86 fat-tailed sheep (Supplemental Table S19) by calculating population differentiation values (F_{ST}) and nucleotide diversity ratios ($\ln(\pi_{\text{Fat-tailed}}/\pi_{\text{Fat-rumped}})$) using VCFtools with a window of 50 kb and a step size of 10 kb (Supplemental Methods).

GWAS of the number of caudal vertebrae in an F_2 population. After mapping and variation calling as detailed above, we performed GWAS analysis of the number of caudal vertebrae using a mixed model in GEMMA software (Zhou and Stephens 2012) (Supplemental Methods). Sex and the first three PCA values calculated by PLINK

were taken as the covariates. The genome-wide significance threshold was set at $-\log_{10}(0.05/\text{Total SNP}) = 8.561$.

Genetic modification in TBXT using CRISPR-Cas9. The sgRNA targeting exon 2 of *TBXT* (Fig. 5F,I) was designed using the online tool (http://www.e-crisp.org/E-CRISP/reannotate_crispr.html) and then cloned into the pX330 vector containing two expression cassettes, a human *Streptococcus pyogenes* (hSpy) Cas9 and the chimeric gRNA. To synthesize sgRNA in vitro, expression vectors were first linearized by digestion with *DraI* and then used as templates to produce sgRNA and Cas9 mRNA using the MEGAshortscriptTM T7 transcription kit (Ambion, Austin, TX, USA) and mMESSAGE mMACHINE® T7 ULTRA transcription kit (Ambion, USA), respectively. Cas9 mRNA and sgRNA were purified using a MEGAclearTM transcription clean-up kit (Ambion, USA) and dissolved in RNase-free water. RNA concentrations were measured using a NanoDrop spectrophotometer (Thermo Fisher Scientific Inc., Wilmington, DE, USA). RNA quality was assessed by agarose gel electrophoresis.

To obtain the designed mutations in *TBXT* through homologous recombination (HR)-mediated repair, we synthesized 123-bp long single-strand DNA oligonucleotide (ssODN) donors, allowing knock-in of two specific mutations, Gly112Trp substitution (C334A) and synonymous mutation (C333G) (Fig. 5I). Finally, 50 ng/μl sgRNA, 100 ng/μl Cas9 mRNA mixture and 100 ng/μl ssODN mixture were prepared using RNase-free water and microinjected into the cytoplasm of Chinese merino zygotes, which were collected through surgical oviduct flushing of donors by estrus synchronization and superovulation. A one-year-old GM079 (male) was selected and mated with the wild-type Chinese Merino ewe, producing 19 offspring with the target mutation C334A and five offspring with an 8-bp indel (Supplemental Table S24).

Validation of the C334A mutation in TBXT. We further genotyped the *TBXT* mutation C334A in the genetically modified sheep and their offspring as well as in 867 sheep from 19 populations with different tail configurations (Supplemental Table S21) by Sanger sequencing. We performed PCR amplifications with the primers *TBXT*-F (5'-ACAAGAAGGTGCAGAGTCACAGGCCCCTC) and *TBXT*-R (GAGCTTCCTGCCCCAAATGACAGATGCC-3') (Supplemental Methods).

Data access

Raw sequencing reads from PacBio, Illumina, Hi-C, RNA-seq and Iso-Seq were deposited in the National Center for Biotechnology Information (NCBI) BioProject database (BioProject; https://www.ncbi.nlm.nih.gov/bioproject/) under the accession numbers PRJNA685905 (Tibetan sheep assembly), PRJNA807094 (Marco Polo sheep assembly), PRJNA807886 (maternal assembly of the F_1-hybrid) and PRJNA808184 (paternal assembly of the F_1-hybrid). The assembly and annotation were archived in the NCBI under the accession numbers GCA_017524585.1 (Tibetan sheep), JAKZEL000000000 (Marco Polo sheep), JALAIW000000000 (maternal haplotype of the F_1-hybrid) and JALAIX000000000 (paternal haplotype of the F_1-hybrid). Raw Illumina resequencing data for 402 individuals (i.e., 74 Tibetan sheep and 328 hybrids), 110 individuals of F_2 population have been submitted to NCBI under the BioProject (PRJNA835294 and PRJNA838735) with the accession numbers SRR19392209-SRR19392610 and SRR19414940-SRR19415049.

Competing interests

The authors declare no competing interests.

Acknowledgments

This study was financially supported by grants from the National Key Research and Development Program-Key Projects (2021YFD1200900), National Natural Science

Foundation of China (Nos. 31825024, 31661143014, 31972527 and 32061133010), the Second Tibetan Plateau Scientific Expedition and Research Program (STEP) (No. 2019QZKK0501), Initiation Fund of Sanya Institute of China Agricultural University (SYND-2022-12), the National Key Project for Cultivation of New Varieties of Genetically Modified Organisms by the Ministry of Agriculture (MOA) of China (No. 2016ZX08008001-002-001) and the Xinjiang Natural Science Foundation-Key Projects (No. 2021D01D13). We thank the farmers in Gannan Tibetan Autonomous Prefecture (Hezuo City, Gansu Province) and Prof. Weimin Wang for their help in sampling, and Professor Yu Jiang and several members of his research group for advice and help in part of the data analyses.

Author Contributions

M.-H. L. and M.-J. L. designed and supervised the study. X. L., S.-G. H., X. W. and D.-X. M. performed the genome data analyses. X. L., W.-R. L., L.-Y. L., Z. Y., C.-X. L., X.-R. P., B. H., Z.-H. L., L. C., performed the laboratory and/or farm work. M.-H. L., M.-J. L., X. L., S.-G. H, W.-R. L., L.-Y. L., Z. Y., F.-H. L., J. Y., Y.-X. X., J. D., Q.-H. Z., X.-L. X., S.-S. X., J.-L. H., X.-Z. D., R. D., Y.-F. C., J.-Y. W., L-M W. and P. Z. prepared the samples or provided help during the sample collection. X. L. and M.-H. L. wrote the manuscript with main contributions from M.-J. L., S.-G. H. and W.-R. L. All authors reviewed and approved the final version of the manuscript.

References

Abbott R, Albach D, Ansell S, Arntzen JW, Baird SJ, Bierne N, Boughman J, Brelsford A, Buerkle CA, Buggs R, et al. 2013. Hybridization and speciation. *J Evol Biol* **26**: 229-246.

Akera T, Chmátal L, Trimm E, Yang K, Aonbangkhen C, Chenoweth DM, Janke C, Schultz RM, Lampson MA. 2017. Spindle asymmetry drives non-Mendelian chromosome segregation. *Science* **358**: 668-672.

840 Akera T, Trimm E, Lampson MA. 2019. Molecular strategies of meiotic cheating by
841 selfish centromeres. *Cell* **178**: 1132-1144. e1110.
842 Alberto FJ, Boyer F, Orozco-terWengel P, Streeter I, Servin B, de Villemereuil P,
843 Benjelloun B, Librado P, Biscarini F, Colli L, et al. 2018. Convergent genomic
844 signatures of domestication in sheep and goats. *Nat Commun* **9**: 1-9.
845 Alexander DH, Novembre J, Lange K. 2009. Fast model-based estimation of ancestry
846 in unrelated individuals. *Genome Res* **19**: 1655-1664.
847 Alexander KF, David AB. 2005. Ovis ammon. *Mamm Species* **773**: 1-15.
848 Arnold ML. 2004. Natural hybridization and the evolution of domesticated, pest and
849 disease organisms. *Mol Ecol* **13**: 997-1007.
850 Barbato M, Hailer F, Orozco-terWengel P, Kijas J, Mereu P, Cabras P, Mazza R,
851 Pirastru M, Bruford MW. 2017. Genomic signatures of adaptive introgression
852 from European mouflon into domestic sheep. *Sci Rep* **7**: 1-13.
853 Bedell JA, Korf I, Gish W. 2000. MaskerAid: a performance enhancement to
854 RepeatMasker. *Bioinformatics* **16**: 1040-1041.
855 Benson G. 1999. Tandem repeats finder: a program to analyze DNA sequences.
856 *Nucleic Acids Res* **27**: 573-580.
857 Benton MJ, Donoghue PC. 2007. Paleontological evidence to date the tree of life. *Mol*
858 *Biol Evol* **24**: 26-53.
859 Blighe K, DeDionisio L, Christie K, Chawes B, Shareef S, Kakouli-Duarte T,
860 Chao-Shern C, Harding V, Kelly R, Castellano L, et al. 2018. Gene editing in
861 the context of an increasingly complex genome. *BMC Genomics* **19**: 1-20.
862 Bredemeyer KR, Harris AJ, Li G, Zhao L, Foley NM, Roelke-Parker M, O'Brien SJ,
863 Lyons LA, Warren WC, Murphy WJ. 2021. Ultracontinuous single haplotype
864 genome assemblies for the domestic cat (Felis catus) and Asian leopard cat
865 (Prionailurus bengalensis). *J Hered* **112**: 165-173.
866 Brown D, Meadowcroft S. 1996. The modern shepherd. Farming Press, Ipswich.
867 Buckingham KJ, McMillin MJ, Brassil MM, Shively KM, Magnaye KM, Cortes A,
868 Weinmann AS, Lyons LA, Bamshad MJ. 2013. Multiple mutant T alleles

cause haploinsufficiency of Brachyury and short tails in Manx cats. *Mamm Genome* **24**: 400-408.

Bunch T, Foote W. 1977. Evolution of the 2n= 54 karyotype of Domestic sheep (Ovis aries). *Ann Genet Sel Anim* **9**: 509-515.

Bunch TD, Wu C, Zhang Y-P, Wang S. 2006. Phylogenetic analysis of snow sheep (Ovis nivicola) and closely related taxa. *J Hered* **97**: 21-30.

Burton JN, Adey A, Patwardhan RP, Qiu R, Kitzman JO, Shendure J. 2013. Chromosome-scale scaffolding of de novo genome assemblies based on chromatin interactions. *Nat Biotechnol* **31**: 1119-1125.

Cao Y-H, Xu S-S, Shen M, Chen Z-H, Gao L, Lv F-H, Xie X-L, Wang X-H, Yang H, Liu C-B, et al. 2021. Historical introgression from wild relatives enhanced climatic adaptation and resistance to pneumonia in sheep. *Mol Biol Evol* **38**: 838-855.

Caro T, Lombardo L, Goldizen A, Kelly M. 1995. Tail-flagging and other antipredator signals in white-tailed deer: new data and synthesis. *Behav Ecol* **6**: 442-450.

Chen W, Zou M, Li Y, Zhu S, Li X, Li J. 2021. Sequencing an F1 hybrid of Silurus asotus and S. meridionalis enabled the assembly of high-quality parental genomes. *Sci Rep* **11**: 1-10.

Chen Z-H, Xu Y-X, Xie X-L, Wang D-F, Aguilar-Gómez D, Liu G-J, Li X, Esmailizadeh A, Rezaei V, Kantanen J, et al. 2021. Whole-genome sequence analysis unveils different origins of European and Asiatic mouflon and domestication-related genes in sheep. *Commun Biol* **4**: 1-15.

Chen ZJ. 2013. Genomic and epigenetic insights into the molecular bases of heterosis. *Nat Rev Genet* **14**: 471-482.

Cheng H, Concepcion GT, Feng X, Zhang H, Li H. 2021. Haplotype-resolved de novo assembly using phased assembly graphs with hifiasm. *Nat Methods* **18**: 170-175.

Cheng H, Zhang Z, Wen J, Lenstra JA, Heller R, Cai Y, Guo Y, Li M, Li R, Li W, et al. 2022. Long divergent haplotypes introgressed from wild sheep are associated with distinct morphological and adaptive characteristics in domestic sheep. bioRxiv 2022.05.17.492311.

Cottone L, Cribbs AP, Khandelwal G, Wells G, Ligammari L, Philpott M, Tumber A, Lombard P, Hookway ES, Szommer T, et al. 2020. Inhibition of Histone H3K27 Demethylases Inactivates Brachyury (TBXT) and Promotes Chordoma Cell Death. *Cancer Res* **80**: 4540–4551.

Danecek P, Auton A, Abecasis G, Albers CA, Banks E, DePristo MA, Handsaker RE, Lunter G, Marth GT, Sherry ST, et al. 2011. The variant call format and VCFtools. *Bioinformatics* **27**: 2156-2158.

de Vos JM, Augustijnen H, Bätscher L, Lucek K. 2020. Speciation through chromosomal fusion and fission in Lepidoptera. *Philos Trans R Soc Lond B Biol Sci* **375**: 20190539.

Deng J, Xie X-L, Wang D-F, Zhao C, Lv F-H, Li X, Yang J, Yu J-L, Shen M, Gao L, et al. 2020. Paternal origins and migratory episodes of domestic sheep. *Curr Biol* **30**: 4085-4095.

Du LX. 2011. Animal Genetic Resources in China. China Agriculture Press, Beijing.

Emms DM, Kelly S. 2019. OrthoFinder: phylogenetic orthology inference for comparative genomics. *Genome Biol* **20**: 1-14.

Feng X, Cheung JPY, Je JS, Cheung PW, Chen S, Yue M, Wang N, Choi VN, Yang X, Song YQ, et al. 2021. Genetic variants of TBX6 and TBXT identified in patients with congenital scoliosis in Southern China. *J Orthop Res* **39**: 971-988.

Goulet BE, Roda F, Hopkins R. 2017. Hybridization in plants: old ideas, new techniques. *Plant Physiol* **173**: 65-78.

Griffiths-Jones S, Moxon S, Marshall M, Khanna A, Eddy SR, Bateman A. 2005. Rfam: annotating non-coding RNAs in complete genomes. *Nucleic Acids Res* **33**: D121-D124.

Haas BJ, Salzberg SL, Zhu W, Pertea M, Allen JE, Orvis J, White O, Buell CR, Wortman JR. 2008. Automated eukaryotic gene structure annotation using EVidenceModeler and the Program to Assemble Spliced Alignments. *Genome Biol* **9**: 1-22.

Han J, Yang M, Guo T, Niu C, Liu J, Yue Y, Yuan C, Yang B. 2019. Two linked TBXT (brachyury) gene polymorphisms are associated with the tailless phenotype in fat-rumped sheep. *Anim Genet* **50**: 772-777.

Han MV, Thomas GW, Lugo-Martinez J, Hahn MW. 2013. Estimating gene gain and loss rates in the presence of error in genome assembly and annotation using CAFE 3. *Mol Biol Evol* **30**: 1987-1997.

Han Z, Cui K, Placek K, Hong N, Lin C, Chen W, Zhao K, Jin W. 2020. Diploid genome architecture revealed by multi-omic data of hybrid mice. *Genome Res* **30**: 1097-1106.

Hassold T, Hunt P. 2001. To err (meiotically) is human: the genesis of human aneuploidy. *Nat Rev Genet* **2**: 280–291.

Haworth K, Putt W, Cattanach B, Breen M, Binns M, Lingaas F, Edwards YH. 2001. Canine homolog of the T-box transcription factor T; failure of the protein to bind to its DNA target leads to a short-tail phenotype. *Mamm Genome* **12**: 212-218.

Hsuchou H, He Y, Kastin AJ, Tu H, Markadakis EN, Rogers RC, Fossier PB, Pan W. 2009. Obesity induces functional astrocytic leptin receptors in hypothalamus. *Brain* **132**: 889-902.

Hu J, Fan J, Sun Z, Liu S. 2020. NextPolish: a fast and efficient genome polishing tool for long-read assembly. *Bioinformatics* **36**:2253-2255.

Hu X-J, Yang J, Xie X-L, Lv F-H, Cao Y-H, Li W-R, Liu M-J, Wang Y-T, Li J-Q, Liu Y-G, et al. 2019. The genome landscape of Tibetan sheep reveals adaptive introgression from argali and the history of early human settlements on the Qinghai–Tibetan Plateau. *Mol Biol Evol* **36**: 283-303.

954 Iannuzzi L, Di Berardino D. 2008. Tools of the trade: diagnostics and research in
955 domestic animal cytogenetics. *J Appl Genet* **49**: 357-366.
956 Jalessi M, Gholami MS, Razmara E, Hassanzadeh S, Sadeghipour A, Jahanbakhshi A,
957 Tabibkhooei A, Bahrami E, Falah M. 2022. Association between TBXT
958 rs2305089 polymorphism and chordoma in Iranian patients identified by a
959 developed T-ARMS-PCR assay. *J Clin Lab Anal* **36**: e24150.
960 Kang HM, Sul JH, Service SK, Zaitlen NA, Kong S-y, Freimer NB, Sabatti C, Eskin
961 E. 2010. Variance component model to account for sample structure in
962 genome-wide association studies. *Nat Genet* **42**: 348-354.
963 Keilwagen J, Wenk M, Erickson JL, Schattat MH, Grau J, Hartung F. 2016. Using
964 intron position conservation for homology-based gene prediction. *Nucleic*
965 *Acids Res* **44**: e89.
966 Kurahashi H, Tsutsumi M, Nishiyama S, Kogo H, Inagaki H, Ohye T. 2012.
967 Molecular basis of maternal age-related increase in oocyte aneuploidy.
968 *Congenit Anom (Kyoto)* **52**: 8-15.
969 Krzywinski M, Schein J, Birol I, Connors J, Gascoyne R, Horsman D, Jones SJ,
970 Marra MA. 2009. Circos: an information aesthetic for comparative genomics.
971 *Genome Res* **19**: 1639-1645.
972 Lagesen K, Hallin P, Rødland EA, Stærfeldt H-H, Rognes T, Ussery DW. 2007.
973 RNAmmer: consistent and rapid annotation of ribosomal RNA genes. *Nucleic*
974 *Acids Res* **35**: 3100-3108.
975 Lauvergne J, Hoogschagen P. 1978. Genetic formulas for the colour in the Texel, the
976 Dutch and the Zwartbles sheep in the Netherlands. *Ann Genet Sel Anim*
977 **10**:343-351.
978 Lawal RA, Martin SH, Vanmechelen K, Vereijken A, Silva P, Al-Atiyat RM,
979 Aljumaah RS, Mwacharo JM, Wu D-D, Zhang Y-P, et al. 2020. The wild
980 species genome ancestry of domestic chickens. *BMC Biol* **18**: 1-18.
981 Li H. 2018. Minimap2: pairwise alignment for nucleotide sequences. *Bioinformatics*
982 **34**: 3094-3100.

983 Li H, Durbin R. 2009. Fast and accurate short read alignment with Burrows–Wheeler
984 transform. *Bioinformatics* **25**: 1754-1760.
985 Li H, Handsaker B, Wysoker A, Fennell T, Ruan J, Homer N, Marth G, Abecasis G,
986 Durbin R, 1000 Genome Project Data Processing Subgroup. 2009. The
987 sequence alignment/map format and SAMtools. *Bioinformatics* **25**:
988 2078-2079.
989 Lowe TM, Eddy SR. 1997. tRNAscan-SE: a program for improved detection of
990 transfer RNA genes in genomic sequence. *Nucleic Acids Res* **25**: 955-964.
991 Luo X, Zhou Y, Zhang B, Zhang Y, Wang X, Feng T, Li Z, Cui K, Wang Z, Luo C, et
992 al. 2020. Understanding divergent domestication traits from the whole-genome
993 sequencing of swamp-and river-buffalo populations. *Natl Sci Rev* **7**: 686-701.
994 Lv F-H, Cao Y-H, Liu G-J, Luo L-Y, Lu R, Liu M-J, Li W-R, Zhou P, Wang X-H,
995 Shen M, et al. 2022. Whole-Genome Resequencing of Worldwide Wild and
996 Domestic Sheep Elucidates Genetic Diversity, Introgression, and
997 Agronomically Important Loci. *Mol Biol Evol* **39**: msab353.
998 Mabry ME, Rowan TN, Pires JC, Decker JE. 2021. Feralization: confronting the
999 complexity of domestication and evolution. *Trends Genet* **37**: 302-305.
1000 Marçais G, Delcher AL, Phillippy AM, Coston R, Salzberg SL, Zimin A. 2018.
1001 MUMmer4: A fast and versatile genome alignment system. *PLoS Comput.*
1002 *Biol* **14**: e1005944.
1003 Martin BL, Kimelman D. 2008. Regulation of canonical Wnt signaling by Brachyury
1004 is essential for posterior mesoderm formation. *Dev Cell* **15**: 121-133.
1005 Mayr B, Krutzler J, Schleger W, Auer H. 1986. A new type of Robertsonian
1006 translocation in the domestic dog. *J Hered* **77**: 127-127.
1007 McClintock B. 1984. The significance of responses of the genome to challenge.
1008 *Science* **226**: 792-801.
1009 McKenna A, Hanna M, Banks E, Sivachenko A, Cibulskis K, Kernytsky A, Garimella
1010 K, Altshuler D, Gabriel S, Daly M, et al. 2010. The Genome Analysis Toolkit:

a MapReduce framework for analyzing next-generation DNA sequencing data. *Genome Res* **20**: 1297-1303.

Meisler MH. 1997. Mutation watch: mouse brachyury (T), the T-box gene family, and human disease. *Mamm Genome* **8**:799-800.

Minh BQ, Schmidt HA, Chernomor O, Schrempf D, Woodhams MD, Von Haeseler A, Lanfear R. 2020. IQ-TREE 2: new models and efficient methods for phylogenetic inference in the genomic era. *Mol Biol Evol* **37**: 1530-1534.

Moran BM, Payne C, Langdon Q, Powell DL, Brandvain Y, Schumer M. 2021. The genomic consequences of hybridization. *Elife* **10**, e69016.

Mori E, Maggini I, Menchetti M. 2014. When quills kill: the defense strategy of the crested porcupine Hystrix cristata L., 1758. *Mammalia* **78**: 229-234.

Mostovoy Y, Levy-Sakin M, Lam J, Lam ET, Hastie AR, Marks P, Lee J, Chu C, Lin C, Džakula Ž, et al. 2016. A hybrid approach for de novo human genome sequence assembly and phasing. *Nat Methods* **13**: 587-590.

Nagao M, Lanjakornsiripan D, Itoh Y, Kishi Y, Ogata T, Gotoh Y. 2014. High Mobility Group Nucleosome□Binding Family Proteins Promote Astrocyte Differentiation of Neural Precursor Cells. *Stem Cells* **32**: 2983-2997.

Nattestad M, Schatz MC. 2016. Assemblytics: a web analytics tool for the detection of variants from an assembly. *Bioinformatics* **32**: 3021-3023.

Nawrocki EP, Eddy SR. 2013. Infernal 1.1: 100-fold faster RNA homology searches. *Bioinformatics* **29**: 2933-2935.

Nikalayevich E, Verlhac M-H. 2021. Selfish centromeres, selfless heterochromatin. *Cell* **184**: 4843-4844.

O'Connor SM, Dawson TJ, Kram R, Donelan JM. 2014. The kangaroo's tail propels and powers pentapedal locomotion. *Biol Lett* **10**: 20140381.

Page SL, Shin J-C, Han J-Y, Andy Choo K, Shaffer LG. 1996. Breakpoint diversity illustrates distinct mechanisms for Robertsonian translocation formation. *Hum Mol Genet* **5**: 1279-1288.

1039 Pan Z, Li S, Liu Q, Wang Z, Zhou Z, Di R, Miao B, Hu W, Wang X, Hu X, et al.
1040 2018. Whole-genome sequences of 89 Chinese sheep suggest role of RXFP2
1041 in the development of unique horn phenotype as response to semi-feralization.
1042 *GigaScience* **7**: giy019.
1043 Pauciullo A, Knorr C, Perucatti A, Iannuzzi A, Iannuzzi L, Erhardt G. 2016.
1044 Characterization of a very rare case of living ewe-buck hybrid using classical
1045 and molecular cytogenetics. *Sci Rep* **6**: 1-8.
1046 Purcell S, Neale B, Todd-Brown K, Thomas L, Ferreira MA, Bender D, Maller J,
1047 Sklar P, De Bakker PI, Daly MJ, et al. 2007. PLINK: a tool set for
1048 whole-genome association and population-based linkage analyses. *Am J Hum*
1049 *Genet* **81**: 559-575.
1050 Randi E. 2008. Detecting hybridization between wild species and their domesticated
1051 relatives. *Mol Ecol* **17**: 285-293.
1052 Rezaei HR, Naderi S, Chintauan-Marquier IC, Taberlet P, Virk AT, Naghash HR,
1053 Rioux D, Kaboli M, Luikart G, et al. 2010. Evolution and taxonomy of the
1054 wild species of the genus Ovis (Mammalia, Artiodactyla, Bovidae). *Mol*
1055 *Phylogenet Evol* **54**: 315-326.
1056 Rice ES, Koren S, Rhie A, Heaton MP, Kalbfleisch TS, Hardy T, Hackett PH,
1057 Bickhart DM, Rosen BD, Ley BV, et al. 2020. Continuous chromosome-scale
1058 haplotypes assembled from a single interspecies F1 hybrid of yak and cattle.
1059 *GigaScience* **9**: giaa029.
1060 Salviano MB, Cursino MS, Zanetti EdS, Abril VV, Duarte JMB. 2017. Intraspecific
1061 chromosome polymorphisms can lead to reproductive isolation and speciation:
1062 an example in red brocket deer (Mazama americana). *Biol Reprod* **96**:
1063 1279-1287.
1064 Schröder O, Lieckfeldt D, Lutz W, Rudloff C, Frölich K, Ludwig A. 2016. Limited
1065 hybridization between domestic sheep and the European mouflon in Western
1066 Germany. *Eur J Wildl Res* **62**: 307-314.

Servant N, Varoquaux N, Lajoie BR, Viara E, Chen C-J, Vert J-P, Heard E, Dekker J, Barillot E. 2015. HiC-Pro: an optimized and flexible pipeline for Hi-C data processing. *Genome Biol* **16**: 1-11.

Sieber M, Freeman AE, Kelley DH. 1988. Relationships between body measurements, body weight, and productivity in Holstein dairy cows. *Journal of Dairy Science* **71**: 3437-3445.

Siniscalchi M, Lusito R, Vallortigara G, Quaranta A. 2013. Seeing left-or right-asymmetric tail wagging produces different emotional responses in dogs. *Curr Biol* **23**: 2279-2282.

Smith B, Aseltine M, Kennedy G. 1997. Beginning Shepherd's Manual, Second Edition. Iowa State University Press, Iowa.

Smith J, Price B, Green J, Weigel D, Herrmann B. 1991. Expression of a Xenopus。homolog of Brachyury (T) is an immediate-early response to mesoderm induction. *Cell* **67**: 79-87.

Song J, Sun L, Xu S, Liu N, Yao Y, Liu Z, Wang W, Rong H, Wang B. 2016. A family with Robertsonian translocation: a potential mechanism of speciation in humans. *Mol Cytogenet* **9**: 1-7.

Stanke M, Diekhans M, Baertsch R, Haussler D. 2008. Using native and syntenically mapped cDNA alignments to improve de novo gene finding. *Bioinformatics* **24**: 637-644.

Stanke M, Schöffmann O, Morgenstern B, Waack S. 2006. Gene prediction in eukaryotes with a generalized hidden Markov model that uses hints from external sources. *BMC Bioinform* **7**: 1-11.

Stelkens R, Seehausen O. 2009. Genetic distance between species predicts novel trait expression in their hybrids. *Evolution* **63**: 884-897.

Sun Y, Lu Z, Zhu X, Ma H. 2020. Genomic basis of homoploid hybrid speciation within chestnut trees. *Nat Commun* **11**: 1-10.

1094 Thomsen P D, Schauser K, Bertelsen M F, Vejlsted M, Grøndahl C, Christensen, K.
1095 2011. Meiotic studies in infertile domestic pig-babirusa hybrids. *Cytogenet*
1096 *Genome Res* **132**: 124-128.
1097 Urasaki N, Takagi H, Natsume S, Uemura A, Taniai N, Miyagi N, Fukushima M,
1098 Suzuki S, Tarora K, Tamaki M, et al. 2017. Draft genome sequence of bitter
1099 gourd (Momordica charantia), a vegetable and medicinal plant in tropical and
1100 subtropical regions. *DNA Res* **24**: 51-58.
1101 Vidale M, Berlioz S, Mohammed R. 2022. Iconographic evidence of hybridisation
1102 between Camelus bactrianus and Camelus dromedarius at second-century AD
1103 Hatra, Iraq. *Antiquity* **96**: 201-207.
1104 Vilella AJ, Severin J, Ureta-Vidal A, Heng L, Durbin R, Birney E. 2009.
1105 EnsemblCompara GeneTrees: Complete, duplication-aware phylogenetic trees
1106 in vertebrates. *Genome Res* **19**: 327-335.
1107 Walker C, Vierck Jr CJ, Ritz LA. 1998. Balance in the cat: role of the tail and effects
1108 of sacrocaudal transection. *Behav Brain Res* **91**: 41-47.
1109 Wang X, Liu J, Niu Y, Li Y, Zhou S, Li C, Ma B, Kou Q, Petersen B, Sonstegard T,
1110 et al. 2018. Low incidence of SNVs and indels in trio genomes of
1111 Cas9-mediated multiplex edited sheep. *BMC Genomics* **19**: 1-8.
1112 Wang X, Miao J, Xia J, Chang T, Guangxin E, Bao J, Jin S, Xu L, Zhang L, Zhu B, et
1113 al. 2018. Identifying novel genes for carcass traits by testing G× E interaction
1114 through genome-wide meta-analysis in Chinese Simmental beef cattle. *Livest*
1115 *Sci* **212**: 75-82.
1116 Wang X, Wang L. 2016. GMATA: an integrated software package for genome-scale
1117 SSR mining, marker development and viewing. *Front Plant Sci* **7**: 1350.
1118 Wang Y, Tang H, DeBarry JD, Tan X, Li J, Wang X, Lee T-h, Jin H, Marler B, Guo
1119 H, et al. 2012. MCScanX: a toolkit for detection and evolutionary analysis of
1120 gene synteny and collinearity. *Nucleic Acids Res* **40**: e49-e49.
1121 Weaver S. 2005. Sheep: small-scale sheep keeping for pleasure and profit. Hobby
1122 Farm Press, Irvine.

Willey JS, Biknevicius AR, Reilly SM, Earls KD. 2004. The tale of the tail: limb function and locomotor mechanics in Alligator mississippiensis. *J Exp Biol* **207**: 553-563.

Wooster C. 2005. Living with Sheep: Everything You Need to Know to Raise Your Own Flock. The Lyons Press, Guilford.

Woronzow N, Korobizgna K, Nadler C, Hofman R, Esalojnitskow T, Gorelow J. 1972. Chromossomi dikich baranow i proisschojdjenije domaschnich owjez. *Lriroda* **3**: 74-81.

Wu B, Shao Y, Chen B, Liu C, Xue Z, Wu P, Li H. 2010. Identification of a novel mouse brachyury (T) allele causing a short tail mutation in mice. *Cell Biochem Biophys* **58**: 129-135.

Wu D-D, Ding X-D, Wang S, Wójcik JM, Zhang Y, Tokarska M, Li Y, Wang M-S, Faruque O, Nielsen R, et al. 2018. Pervasive introgression facilitated domestication and adaptation in the Bos species complex. *Nat Ecol Evol* **2**: 1139-1145.

Xia B, Zhang W, Wudzinska A, Huang E, Brosh R, Pour M, Miller A, Dasen JS, Maurano MT, Kim SY, et al. 2021. The genetic basis of tail-loss evolution in humans and apes. bioRxiv 2021.09.14.460388.

Xiao Y, Jiang S, Cheng Q, Wang X, Yan J, Zhang R, Qiao F, Ma C, Luo J, Li W, et al. 2021. The genetic mechanism of heterosis utilization in maize improvement. *Genome Biol* **22**: 1-29.

Xu B, Xie X. 2016. Neurotrophic factor control of satiety and body weight. *Nat Rev Neurosci* **17**: 282-292.

Yang J, Lee SH, Goddard ME, Visscher PM. 2011. GCTA: a tool for genome-wide complex trait analysis. *Am J Hum Genet* **88**:76-82.

Yang J, Manolio TA, Pasquale LR, Boerwinkle E, Caporaso N, Cunningham JM, De Andrade M, Feenstra B, Feingold E, Hayes MG, et al. 2011. Genome partitioning of genetic variation for complex traits using common SNPs. *Nat Genet* **43**: 519-525.

1152 Yang Y, Wang Y, Zhao Y, Zhang X, Li R, Chen L, Zhang G, Jiang Y, Qiu Q, Wang
1153 W, et al. 2017. Draft genome of the Marco Polo Sheep (Ovis ammon polii).
1154 *GigaScience* **6**: 1-7.
1155 Yang Z. 2007. PAML 4: phylogenetic analysis by maximum likelihood. *Mol. Biol.*
1156 *Evol.* **24**: 1586-1591.
1157 Young JW, Russo GA, Fellmann CD, Thatikunta MA, Chadwell BA. 2015. Tail
1158 function during arboreal quadrupedalism in squirrel monkeys (Saimiri
1159 boliviensis) and tamarins (Saguinus oedipus). *J Exp Zool A Ecol Genet*
1160 *Physiol* **323**: 556-566.
1161 Zhou X, Stephens M. 2012. Genome-wide efficient mixed-model analysis for
1162 association studies. *Nat Genet* **44**: 821-824.
1163 Zhou Z, Li M, Cheng H, Fan W, Yuan Z, Gao Q, Xu Y, Guo Z, Zhang Y, Hu J, et al.
1164 2018. An intercross population study reveals genes associated with body size
1165 and plumage color in ducks. *Nat Commun* **9**: 1-10.
1166

Figure Legends

Figure 1. Research framework, hybridization scheme, karyotypes and chromosomal painting, statistics of homologs and gene families, phylogenetic tree and synteny landscape.

(A) Roadmap of initiation, technical systems, analysis and experiments, the results and purposes of this study. **(B**) The wild (the Marco Polo subspecies of argali, *O. ammon polii*)-domestic sheep (Tibetan sheep) hybridization scheme. The F_1-hybrid is subsequently backcrossed to *O. aries* to produce the progenies, and later hybrid generations are produced by intercrossing and backcrossing. (**C**) Karyotypes and chromosomal painting of Tibetan sheep, argali and their F_1-hybrid. DNA probes (*GNAQ*: green signal; *STK39*: red signal) were used to label the long arm and short arm of Chromosome 2 and two acrocentric chromosomes. DNA was stained with 4,6-diamidino-2-phenylindole (DAPI, blue). **(D**) Number of homologs among the Marco Polo subspecies of argali (*O. ammon polii*), sheep (*O. aries*) and goat (*C. hircus*). **(E**) Proportions of different gene numbers in 19,917 gene families in the nine mammal species. **(F**) Phylogenetic tree of nine mammal species based on 10,043 single-copy orthologous genes. Numbers in green to the right of nodes are the divergence times (MYA, million years ago) and their 95% confidence intervals (95% CIs). Values next to the branches represent the numbers of gene family expansions/contractions. **(G**) Genome-wide syntenic relationship among goat (*C. hircus*), sheep (*O. aries*), the Marco Polo subspecies of argali (*O. ammon polii*) and the argali-domestic sheep F_1-hybrid. Syntenic blocks involved in chromosome fusion are marked with colored ribbons.

Figure 2. Evolution of three metacentric chromosomes of domestic sheep and the proposed molecular basis of fertility for the F_1 hybrid. (A) Repeated sequences surrounding the breakpoints on the chromosomes involved in chromosome fusions in goat (*C. hircus*), argali (*O. ammon polii*) and domestic sheep (*O. aries*). **(B**) Schematic representation of chromosomal segregation and pairing (metacentric

Chromosome 2 of domestic sheep and two acrocentric pseudochromosomes LG04 and LG07 from argali) during hybridization between argali (*O. ammon poli*) and Tibetan sheep (*O. aries*). Six di erent types of zygotes can be produced by the F_1-hybrid, giving only one normal and one balanced embryo after fertilization with domestic sheep. **(C**) Proposed molecular mechanisms underlying the preference of F_1-hybrid oocytes to generate gametes with 27 chromosomes rather than 28 chromosomes. That is, selfish centromeres (red/yellow circles) prefer the egg side when attached to the metaphase I spindle (purple) (Nikalayevich et al. 2021). Chromosomes are in blue/pink, oocyte cytoplasm is in gray, and the zone of cortical proximity is in darker gray.

Figure 3. Genetic structure and genetic diversity of Tibetan sheep, argali and their hybrids. (A) Plots of principal component analysis (principal components 1 and 2) for 425 individuals. **(B**) Nucleotide diversity of argali, Tibetan sheep and their hybrids. **(C**) Population genetic structure of argali, Tibetan sheep and their hybrids inferred using the ADMIXTURE program. The vertical solid line indicated the separations between argali, Tibetans sheep and their hybrids.

Figure 4. Identification of candidate genes related to the tail length and body weight of domestic sheep. (A, **D**) Manhattan and quantile-quantile (Q-Q) plots of association signals for the traits of tail length and body weight. The two dashed lines colored gray and green represent two significant thresholds with –log(*P* value) = 8.88 and 6, respectively. SNPs near the peaks with different significant values are marked in red [maximum $-\log_{10}(P)$ value] or orange [$-\log_{10}(P) \geq 7$], and brown [$7 > -\log_{10}(P) \geq 6$]. Functional genes surrounding the peaks are indicated by red (*TBXT* with the most significant signal) or green (other genes) boxes. **(B**, **E**) Linkage disequilibrium (LD) plots in the regions surrounding the *TBXT* and *HMGN1* genes. **(C**, **F**) Boxplots for the tail length associated with SNP (Chr8: 88,341,610 C/A) and for the body weight associated with SNP (Chr17: 26,391,397 T/G). The lines in boxes denote the

median values; box limits are the upper and lower quartiles, and whiskers show the range of the data; *n* indicates the number of individuals with the same genotype. Significance of differences between the phenotypic values (*$P < 0.05$; **$P < 0.01$) was determined by the Mann-Whitney *U* test.

Figure 5. Genome-wide selection sweep test, genome-wide association study analysis and functional validation of the *TBXT* gene. (**A**) Computerized tomography (CT) scanning of the caudal vertebrae number for fat-rumped (Kazakh, Duolang, Bashiba and Bayinbuluke) and fat-tailed (Hetian and Cele Black) sheep. **(B**) Boxplots for the number of caudal vertebrae between fat-rumped and fat-tailed sheep breeds. **(C**) Genome-wide selection sweep tests (the F_{ST} and π-ratio-based methods) for the tail configuration between fat-rumped and fat-tailed sheep breeds. **(D**) Calculation of Tajima's *D*, π and F_{ST} values for SNPs in the candidate genomic region Chr. 8: 87.56–87.88 Mb between fat-rumped and fat-tailed sheep breeds. **(E**) Amino acid (i.e., p. G112W in the *TBXT* gene) alternation among different mammalian species. **(F**) Manhattan and quantile-quantile (Q-Q) plots of association signals for the tail length and the number of caudal vertebrae in domestic sheep. The dashed line represents the significance threshold ($-\log_{10}(0.05/\text{total SNPs}) = 8.56$). The gene structure of the *TBXT* gene is shown in green, and the exon regions are shown in blue at the bottom. **(G**) Boxplots for the tail length and the number of caudal vertebrae associated with the three genotypes of c.334C>A in *TBXT* in the F_2 intercross population of 110 individuals. **(H**) Different phenotypes in the tail configuration for individuals with the CC and AA genotypes of c.334C>A in *TBXT*; picture credit: Wen-Rong Li. **(I**) Sequences of sgRNA targeting exon 2 of the *TBXT* gene and 123-bp single-strand DNA oligonucleotides (ssODNs) for homologous recombination-mediated repair in CRISPR-Cas9 experimentation. **(J**) Target sequences in wild-type (WT) and 19 mosaic mutant merino sheep. Target mutations are indicated in red bold font. **(K**) Different phenotypes of the tail configuration for WT and mutant merino sheep (GM079); picture credit: Wen-Rong Li. **(L**) CT

scanning of the tail configuration for WT, GM079 and the offspring of GM079. **(M**) Boxplots for the tail length and the number of caudal vertebrae of the 19 WT sheep, 14 C334A target mutation (TM) merino sheep and six sheep with a short indel (KO) in the *TBXT* gene. **(N**) Boxplots for the number of caudal vertebrae of the 19 WT sheep and 24 offspring of GM079 (i.e., 19 heterozygotes with the C334A target (TM/+) and five heterozygotes with an 8-bp deletion (KO/+)).

1261 **Table 1**. Genome assembly and annotation statistics for Tibetan sheep (*O. aries*),
1262 argali (*O. ammon polii*) and the F_1 hybrid (*O. ammon polii* × *O. aries*).
1263

Genomic features	***O. aries***	***O. ammon polii***	***O. ammon polii* × *O. aries* (the F_1-hybrid; *n* = 27)**	***O. ammon polii* × *O. aries* (the F_1-hybrid; *n* = 28)**
Assembly size (bp)	2,653,843,355	2,664,280,018	2,898,997,297	2,710,908,005
Number of chromosomes	27	29	27	28
Genome in chromosomes	99.85%	99.79%	95.85%	97.64%
Number of scaffolds	106	136	165	114
Scaffold N50 (bp)	95,403,819	92,548,278	101,515,600	102,897,427
Number of contigs	128	174	210	177
Contig N50 (bp)	77,474,290	77,943,461	77,913,213	80,500,000
GC content	41.95%	41.96%	43.96%	42.83%
Annotated protein-coding genes (*n*)	20,919	20,916	21,078	20,363
Mean gene length (kb)	47.73	48.63	47.65	47.17
Repeat sequences	45.16%	45.42%	50.38%	46.98%

1264

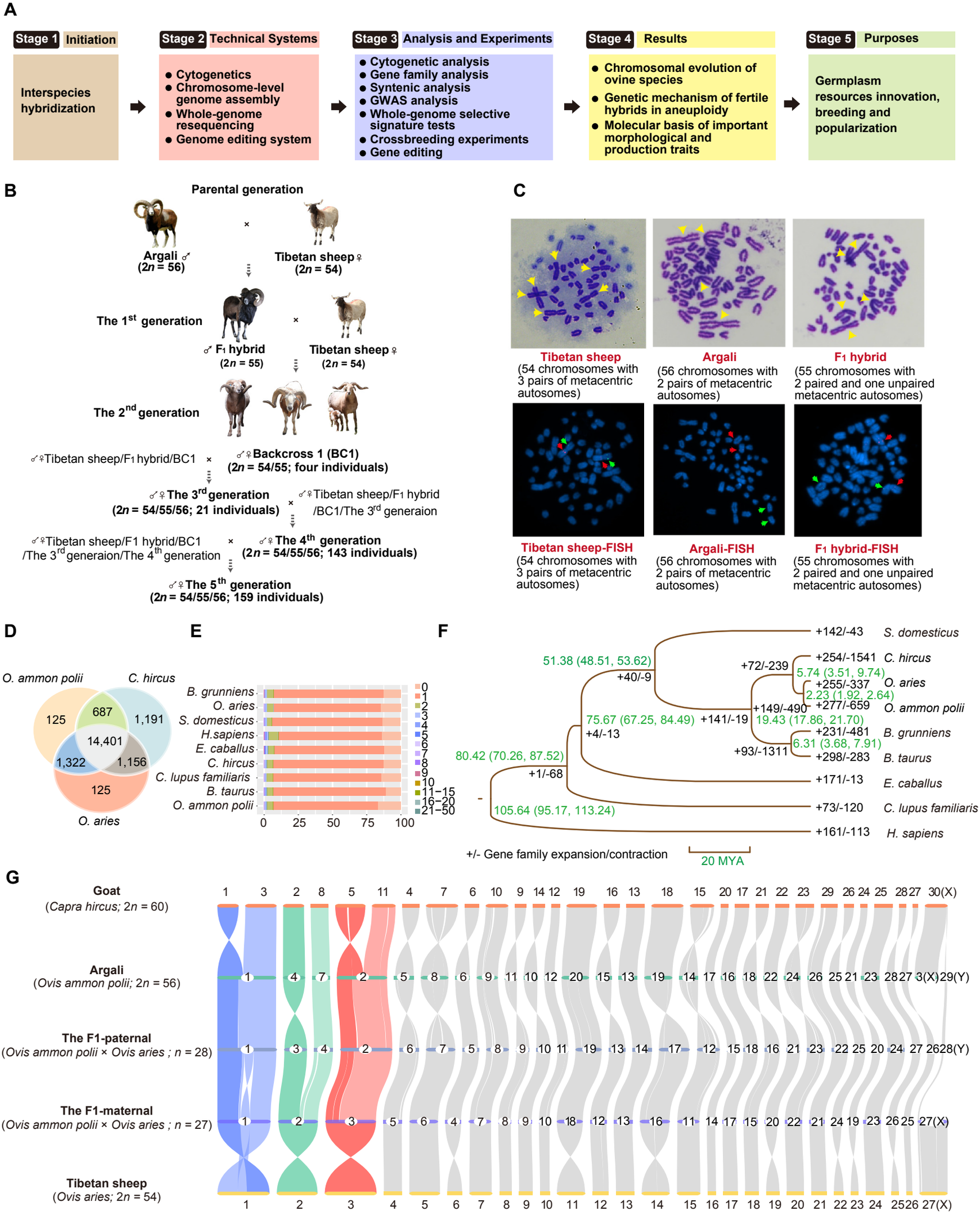
A
Stage 1 Initiation
Interspecies hybridization
Stage 2 Technical Systems
Cytogenetics
Chromosome-level genome assembly
Whole-genome resequencing
Genome editing system
Stage 3 Analysis and Experiments
Cytogenetic analysis
Gene family analysis
Syntenic analysis
GWAS analysis
Whole-genome selective signature tests
Crossbreeding experiments
Gene editing
Stage 4 Results
Chromosomal evolution of ovine species
Genetic mechanism of fertile hybrids in aneuploidy
Molecular basis of important morphological and production traits
Stage 5 Purposes
Germplasm resources innovation, breeding and popularization
B
Parental generation
Argali ♂ (2n = 56)
Tibetan sheep ♀ (2n = 54)
The 1st generation
♂ F1 hybrid (2n = 55)
Tibetan sheep ♀ (2n = 54)
The 2nd generation
♂♀Tibetan sheep/F1 hybrid/BC1
♂♀Backcross 1 (BC1) (2n = 54/55; four individuals)
♂♀The 3rd generation (2n = 54/55/56; 21 individuals)
♂♀Tibetan sheep/F1 hybrid /BC1/The 3rd generaion
♂♀Tibetan sheep/F1 hybrid/BC1 /The 3rd generaion/The 4th generation
♂♀The 4th generation (2n = 54/55/56; 143 individuals)
♂♀The 5th generation (2n = 54/55/56; 159 individuals)
C
Tibetan sheep (54 chromosomes with 3 pairs of metacentric autosomes)
Argali (56 chromosomes with 2 pairs of metacentric autosomes)
F1 hybrid (55 chromosomes with 2 paired and one unpaired metacentric autosomes)
Tibetan sheep-FISH (54 chromosomes with 3 pairs of metacentric autosomes)
Argali-FISH (56 chromosomes with 2 pairs of metacentric autosomes)
F1 hybrid-FISH (55 chromosomes with 2 paired and one unpaired metacentric autosomes)
D
O. ammon polii
C. hircus
O. aries
125
687
1,191
14,401
1,322
1,156
125
E
B. grunniens
O. aries
S. domesticus
H.sapiens
E. caballus
C. hircus
C. lupus familiaris
B. taurus
O. ammon polii
0 25 50 75 100
0 1 2 3 4 5 6 7 8 9 10 11–15 16–20 21–50
F
51.38 (48.51, 53.62)
+40/-9
75.67 (67.25, 84.49)
+4/-13
80.42 (70.26, 87.52)
+1/-68
105.64 (95.17, 113.24)
+72/-239
+141/-19
+149/-490
19.43 (17.86, 21.70)
+277/-659
+93/-1311
5.74 (3.51, 9.74)
2.23 (1.92, 2.64)
6.31 (3.68, 7.91)
+142/-43 S. domesticus
+254/-1541 C. hircus
+255/-337 O. aries
+231/-481 B. grunniens
+298/-283 B. taurus
+171/-13 E. caballus
+73/-120 C. lupus familiaris
+161/-113 H. sapiens
+/- Gene family expansion/contraction
20 MYA
G
Goat (Capra hircus; 2n = 60)
Argali (Ovis ammon polii; 2n = 56)
The F1-paternal (Ovis ammon polii × Ovis aries ; n = 28)
The F1-maternal (Ovis ammon polii × Ovis aries ; n = 27)
Tibetan sheep (Ovis aries; 2n = 54)
1 3 2 8 5 11 4 7 6 10 9 14 12 19 16 13 18 15 20 17 21 22 23 29 26 24 25 28 27 30(X)
1 4 7 2 5 8 6 9 11 10 12 20 15 13 19 14 17 16 18 22 24 26 25 21 23 28 27 3(X) 29(Y)
1 3 4 2 6 7 5 8 9 10 11 19 13 14 17 12 15 18 16 21 23 22 25 20 24 27 26 28(Y)
1 2 3 5 6 4 7 8 9 10 18 12 13 16 11 14 17 15 20 22 21 24 19 23 26 25 27(X)
1 2 3 4 5 6 7 8 9 10 11 12 13 14 15 16 17 18 19 20 21 22 23 24 25 26 27(X)

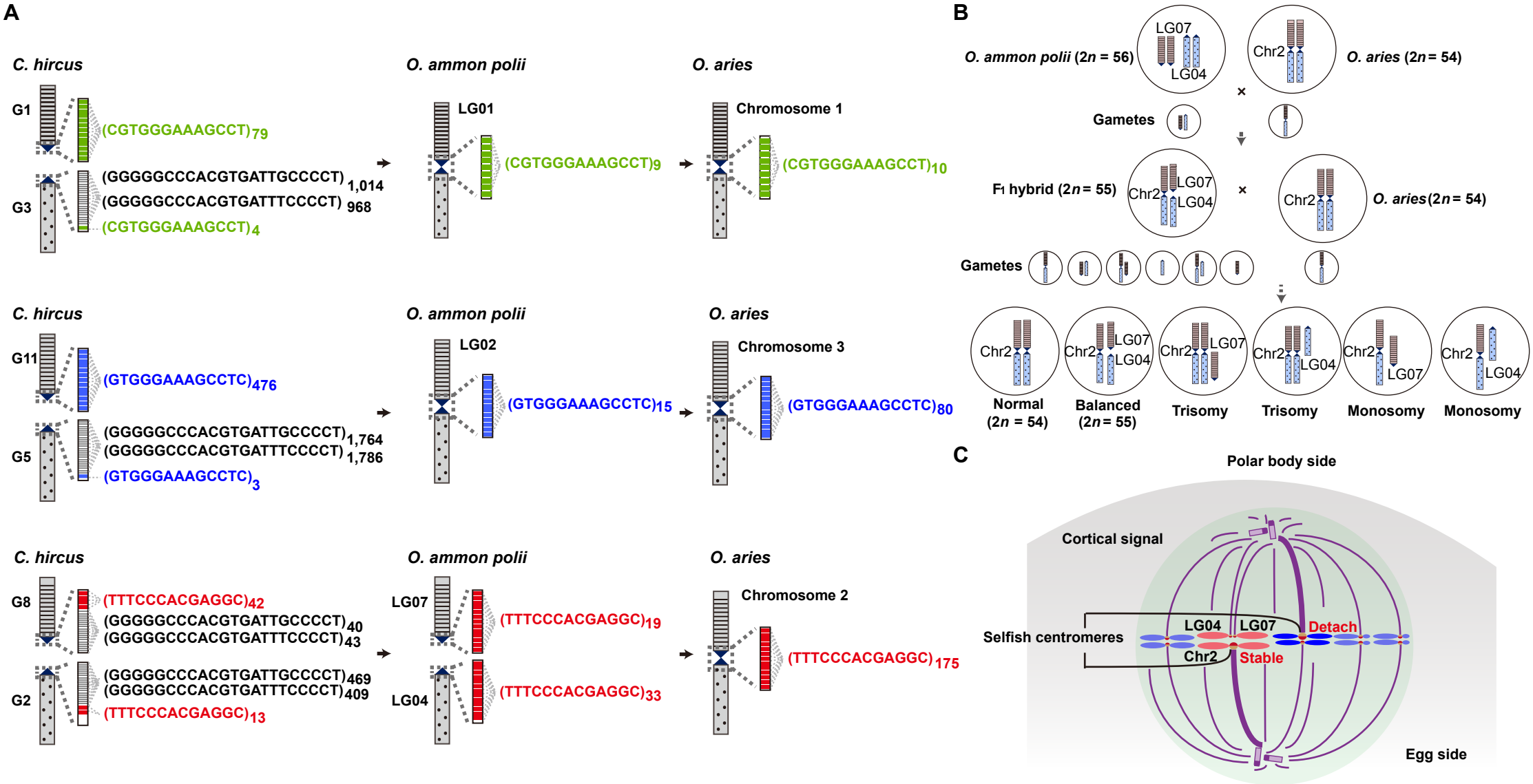
A
C. hircus
O. ammon polii
O. aries
G1
(CGTGGGAAAGCCT)79
G3
(GGGGGCCCACGTGATTGCCCCT) 1,014
(GGGGGCCCACGTGATTTCCCCT) 968
(CGTGGGAAAGCCT)4
LG01
(CGTGGGAAAGCCT)9
Chromosome 1
(CGTGGGAAAGCCT)10
G11
(GTGGGAAAGCCTC)476
G5
(GGGGGCCCACGTGATTGCCCCT) 1,764
(GGGGGCCCACGTGATTTCCCCT) 1,786
(GTGGGAAAGCCTC)3
LG02
(GTGGGAAAGCCTC)15
Chromosome 3
(GTGGGAAAGCCTC)80
G8
(TTTCCCACGAGGC)42
(GGGGGCCCACGTGATTGCCCCT)40
(GGGGGCCCACGTGATTTCCCCT)43
G2
(GGGGGCCCACGTGATTGCCCCT)469
(GGGGGCCCACGTGATTTCCCCT)409
(TTTCCCACGAGGC)13
LG07
(TTTCCCACGAGGC)19
LG04
(TTTCCCACGAGGC)33
Chromosome 2
(TTTCCCACGAGGC)175
B
O. ammon polii (2n = 56)
LG07
LG04
Chr2
O. aries (2n = 54)
Gametes
F1 hybrid (2n = 55)
Normal (2n = 54)
Balanced (2n = 55)
Trisomy
Trisomy
Monosomy
Monosomy
C
Polar body side
Cortical signal
Selfish centromeres
LG04
LG07
Detach
Chr2
Stable
Egg side

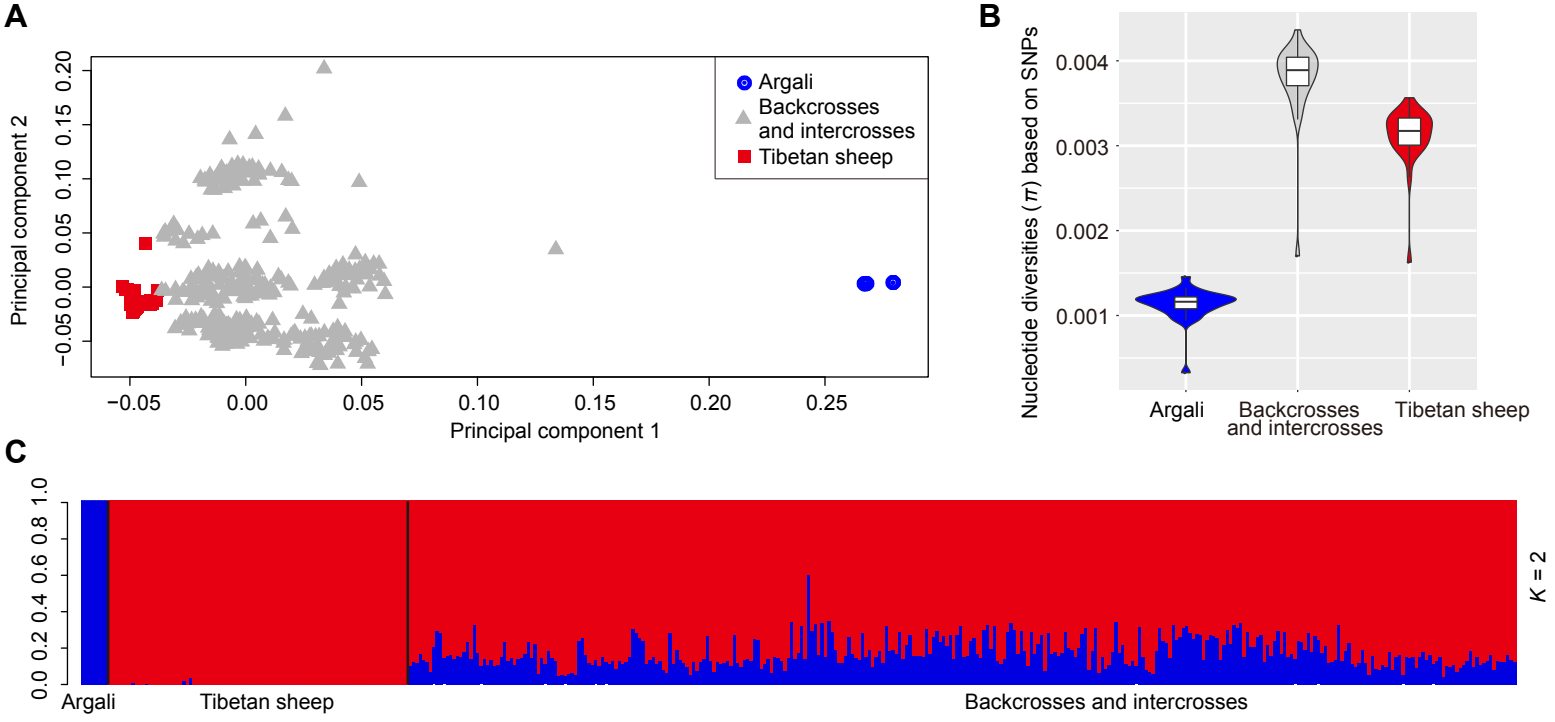
A
Principal component 2
−0.05
0.00
0.05
0.10
0.15
0.20
Principal component 1
−0.05
0.00
0.05
0.10
0.15
0.20
0.25
Argali
Backcrosses and intercrosses
Tibetan sheep
B
Nucleotide diversities (π) based on SNPs
0.001
0.002
0.003
0.004
Argali
Backcrosses and intercrosses
Tibetan sheep
C
0.0
0.2
0.4
0.6
0.8
1.0
K = 2
Argali
Tibetan sheep
Backcrosses and intercrosses

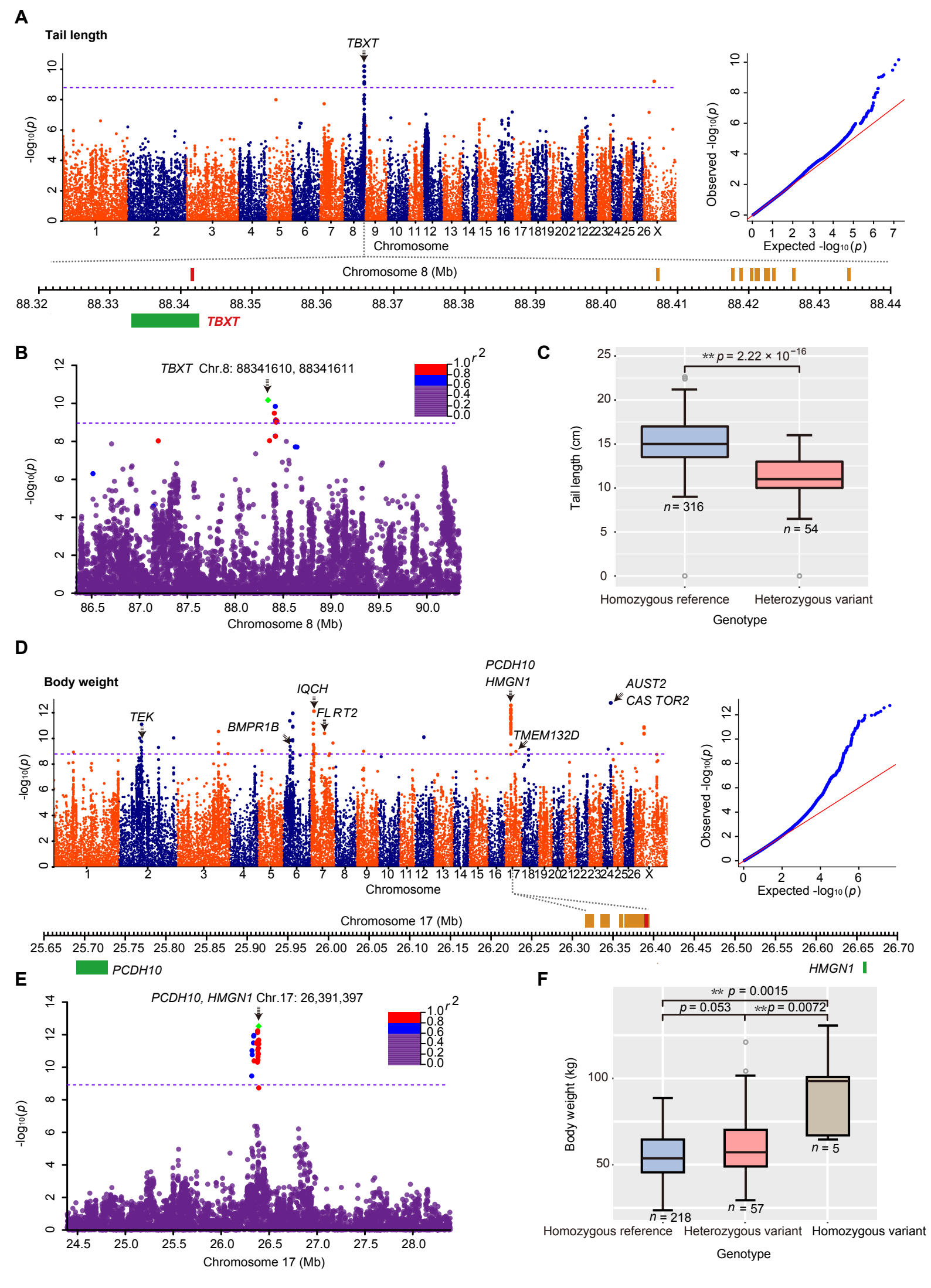
A
Tail length
TBXT
-log10(p)
Chromosome
Observed -log10(p)
Expected -log10(p)
Chromosome 8 (Mb)
TBXT
B
TBXT Chr.8: 88341610, 88341611
r2
Chromosome 8 (Mb)
C
** p = 2.22 × 10−16
Tail length (cm)
n = 316
n = 54
Homozygous reference
Heterozygous variant
Genotype
D
Body weight
TEK
BMPR1B
IQCH
FLRT2
PCDH10
HMGN1
TMEM132D
AUST2
CAS TOR2
Chromosome
Chromosome 17 (Mb)
PCDH10
HMGN1
E
PCDH10, HMGN1 Chr.17: 26,391,397
Chromosome 17 (Mb)
F
** p = 0.0015
p = 0.053
**p = 0.0072
Body weight (kg)
n = 218
n = 57
n = 5
Homozygous reference
Heterozygous variant
Homozygous variant
Genotype

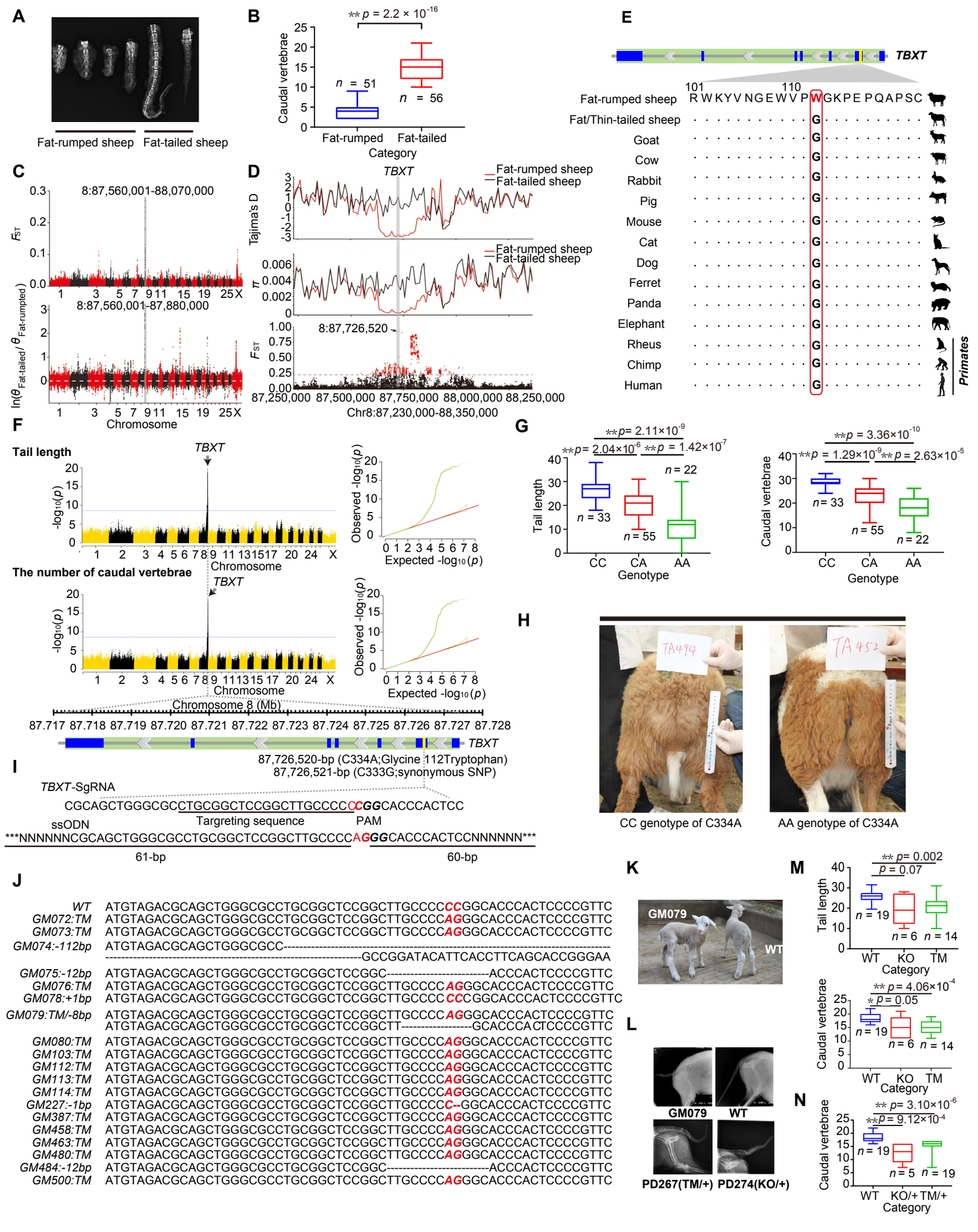
A
Fat-rumped sheep
Fat-tailed sheep
B
** p = 2.2 × 10-16
Caudal vertebrae
n = 51
n = 56
Fat-rumped
Fat-tailed
Category
C
8:87,560,001-88,070,000
FST
8:87,560,001-87,880,000
ln(θFat-tailed/θFat-rumped)
Chromosome
D
TBXT
Fat-rumped sheep
Fat-tailed sheep
Tajima's D
π
8:87,726,520
FST
87,250,000 87,500,000 87,750,000 88,000,000 88,250,000
Chr8:87,230,000-88,350,000
E
TBXT
101
110
Fat-rumped sheep R W K Y V N G E W V P W G K P E P Q A P S C
Fat/Thin-tailed sheep
Goat
Cow
Rabbit
Pig
Mouse
Cat
Dog
Ferret
Panda
Elephant
Rheus
Chimp
Human
Primates
F
Tail length
TBXT
-log10(p)
Chromosome
Observed -log10(p)
Expected -log10(p)
The number of caudal vertebrae
TBXT
-log10(p)
Chromosome
Observed -log10(p)
Expected -log10(p)
Chromosome 8 (Mb)
87.717 87.718 87.719 87.720 87.721 87.722 87.723 87.724 87.725 87.726 87.727 87.728
TBXT
G
**p= 2.11×10-9
**p= 2.04×10-6
**p = 1.42×10-7
Tail length
n = 33
n = 55
n = 22
CC
CA
AA
Genotype
**p = 3.36×10-10
**p = 1.29×10-9
**p = 2.63×10-5
Caudal vertebrae
n = 33
n = 55
n = 22
CC
CA
AA
Genotype
H
TA494
TA452
CC genotype of C334A
AA genotype of C334A
I
87,726,520-bp (C334A;Glycine 112Tryptophan)
87,726,521-bp (C333G;synonymous SNP)
TBXT-SgRNA
CGCAGCTGGGCGCCTGCGGCTCCGGCTTGCCCCCCGGCACCCACTCC
Targreting sequence
PAM
ssODN
NNNNNNCGCAGCTGGGCGCCTGCGGCTCCGGCTTGCCCCAGGGCACCCACTCCNNNNNN
61-bp
60-bp
J
WT ATGTAGACGCAGCTGGGCGCCTGCGGCTCCGGCTTGCCCCCCGGCACCCACTCCCCGTTC
GM072:TM ATGTAGACGCAGCTGGGCGCCTGCGGCTCCGGCTTGCCCCAGGGCACCCACTCCCCGTTC
GM073:TM ATGTAGACGCAGCTGGGCGCCTGCGGCTCCGGCTTGCCCCAGGGCACCCACTCCCCGTTC
GM074:-112bp ATGTAGACGCAGCTGGGCGCC----------GCCGGATACATTCACCTTCAGCACCGGGAA
GM075:-12bp ATGTAGACGCAGCTGGGCGCCTGCGGCTCCGGC----------ACCCACTCCCCGTTC
GM076:TM ATGTAGACGCAGCTGGGCGCCTGCGGCTCCGGCTTGCCCCAGGGCACCCACTCCCCGTTC
GM078:+1bp ATGTAGACGCAGCTGGGCGCCTGCGGCTCCGGCTTGCCCCCCGGCACCCACTCCCCGTTC
GM079:TM/-8bp ATGTAGACGCAGCTGGGCGCCTGCGGCTCCGGCTTGCCCCAGGGCACCCACTCCCCGTTC
ATGTAGACGCAGCTGGGCGCCTGCGGCTCCGGCTT----------GCACCCACTCCCCGTTC
GM080:TM ATGTAGACGCAGCTGGGCGCCTGCGGCTCCGGCTTGCCCCAGGGCACCCACTCCCCGTTC
GM103:TM ATGTAGACGCAGCTGGGCGCCTGCGGCTCCGGCTTGCCCCAGGGCACCCACTCCCCGTTC
GM112:TM ATGTAGACGCAGCTGGGCGCCTGCGGCTCCGGCTTGCCCCAGGGCACCCACTCCCCGTTC
GM113:TM ATGTAGACGCAGCTGGGCGCCTGCGGCTCCGGCTTGCCCCAGGGCACCCACTCCCCGTTC
GM114:TM ATGTAGACGCAGCTGGGCGCCTGCGGCTCCGGCTTGCCCCAGGGCACCCACTCCCCGTTC
GM227:-1bp ATGTAGACGCAGCTGGGCGCCTGCGGCTCCGGCTTGCCCCC--GGCACCCACTCCCCGTTC
GM387:TM ATGTAGACGCAGCTGGGCGCCTGCGGCTCCGGCTTGCCCCAGGGCACCCACTCCCCGTTC
GM458:TM ATGTAGACGCAGCTGGGCGCCTGCGGCTCCGGCTTGCCCCAGGGCACCCACTCCCCGTTC
GM463:TM ATGTAGACGCAGCTGGGCGCCTGCGGCTCCGGCTTGCCCCAGGGCACCCACTCCCCGTTC
GM480:TM ATGTAGACGCAGCTGGGCGCCTGCGGCTCCGGCTTGCCCCAGGGCACCCACTCCCCGTTC
GM484:-12bp ATGTAGACGCAGCTGGGCGCCTGCGGCTCCGGC----------ACCCACTCCCCGTTC
GM500:TM ATGTAGACGCAGCTGGGCGCCTGCGGCTCCGGCTTGCCCCAGGGCACCCACTCCCCGTTC
K
GM079
WT
L
GM079
WT
PD267(TM/+)
PD274(KO/+)
M
** p= 0.002
p = 0.07
Tail length
n = 19
n = 6
n = 14
WT
KO
TM
Category
** p = 4.06×10-4
* p = 0.05
Caudal vertebrae
n = 19
n = 6
n = 14
WT
KO
TM
Category
N
** p= 3.10×10-6
**p= 9.12×10-4
Caudal vertebrae
n = 19
n = 5
n = 19
WT
KO/+
TM/+
Category